Dynamics, Spectra, and Relaxation Phenomena of Excess Electrons in Clusters*

ROBERT N. BARNETT,[a] UZI LANDMAN,[a]** GUNARETNAM RAJAGOPAL,[a] AND ABRAHAM NITZAN[b]

[a]School of Physics, Georgia Institute of Technology, Atlanta, GA 30332, USA

[b]School of Chemistry, Raymond and Beverly Sackler Faculty of Exact Sciences, Tel Aviv University, Ramat Aviv 69978, Tel Aviv, Israel

(*Received 14 May 1989*)

Abstract. In this paper, we review quantum simulation methods for studies of coupled quantum-classical systems and their applications in investigations of dynamics, spectra, and relaxation phenomena of excess electrons in polar molecular and ionic clusters.

1. INTRODUCTION

Recent experimental[1-10] and theoretical[11-36] investigations of nonreactive electron attachment to small clusters open new avenues for studies of electron localization and solvation in atomic and molecular systems and of the general issues of size effects on chemical and physical phenomena. Of particular interest in this context are questions pertaining to the modes[17-33,35,36] and dynamical mechanisms[32] of electron localization in finite aggregates and their spectroscopic consequences[29-35] and of the minimal cluster sizes which sustain bound states of an excess electron.[19,20,27,28,35]

Experimentally, negatively charged gas-phase clusters (polar molecular clusters of water,[1,2,4-6] $(H_2O)_n^-$, and ammonia,[3] $(NH_3)_n^-$, and ionic clusters,[8-10] (Na_nCl_{n-1})), have been prepared, and their mass-dependent abundance has been investigated using time-of-flight mass spectroscopy. In addition, using photoelectron spectroscopy, the excess electron binding energies have been measured for water $(H_2O)_n^-$ (for n in the range 2 to 40)[6] and alkali-halide clusters[10] ((Na_nCl_{n-1}) and (Na_nF_{n-1}), for $2 \leqq n \leqq 40$). Furthermore, measurements of the optical spectra of negatively charged alkali-halide clusters are currently underway.[10c,d] The main observations pertaining to polar molecular clusters may be summarized as follows:

(1) The water dimer constitutes the smallest water cluster which attaches an electron, resulting in a weakly bound $(H_2O)_2^-$ state with an estimated binding energy of ~ 17 meV (from field detachment experiments[3]) or ~ 30 meV (from photoelectron spectroscopy[6]).

(2) Strongly bound $(H_2O)_n^-$ clusters were observed[1-6] for $n \geqq 11$, while for $(NH_3)_n^-$ the minimum cluster size detected[3] is ~ 35. In the case of water, nonreactive electron localization in the clusters was experimentally documented to originate either from electron binding during the cluster nucleation process[1-4,6] or by electron attachment to preexisting clusters.[2,5]

(3) The stable $(H_2O)_n^-$ clusters ($n \geqq 11$) are characterized by a large electron vertical binding energy which varies monotonically with cluster size[6] (-0.75 eV for $n = 11$ to -1.12 eV for $n = 19$).

On the theoretical front, early investigations of negatively charged clusters employed the methods of quantum chemistry for calculations of the electronic structure.[11,12,14,15] These calculations were limited to small clusters (up to ~ 10 water[11,12] or 3–5 alkali-halide molecules[14,15]) and were performed mostly for a restricted set of nuclear configurations. The recent development and application of the quantum-path integral molecular dynamics (QUPID) method,[18-20] the use[29,30,32,33] of the fast Fourier transform (FFT) technique for solution of the Schrödinger equation,[29,30,32-36] and the time-dependent self-consistent field (TDSCF) method[29,30,32,33,37,38] add a new dimension to the research of excess electron

* We dedicate this paper to Professor Joshua Jortner, a teacher, colleague, and friend, whose seminal contributions to our understanding of solvation phenomena and spectroscopy, his insight and relentless scientific endeavors provide an inspiration for our research.

** Author to whom correspondence should be addressed.

interaction with finite atomic and molecular aggregates.[19,20] Using these methods, in conjunction with well-tested interatomic and intermolecular potentials[39-41] and pseudopotentials[16-26,34,35,42] for the description of the interaction of the excess electron with the atomic or molecular constituents of the cluster, yields a wealth of information about the equilibrium, finite temperature, energetics, structure,[17-35] and spectroscopy[29-33] of these systems and about the dynamics and mechanisms[32,33] of excess electron attachment, localization, migration, and solvation in clusters. The main findings from these studies pertaining to electron localization in polar molecular clusters may be summarized as follows:

(1) The localization mode of an excess electron in a polar molecular cluster depends on the cluster size and chemical constituents. For water clusters, $(H_2O)_n^-$, in the size range $11 \leqq n < 64$, the electron is relatively strongly bound in a surface state, while for the larger clusters ($32 \leqq n < 64$) a gradual transition to internal solvation occurs.[23-27] Attachment of the excess electron to small clusters, $n < 10$, is in a diffuse weakly bound surface state.[17,24]

(2) The onset of stable well-bound electron attachment to ammonia clusters, $(NH_3)_n^-$, occurs via internal localization, requiring $n \gtrsim 32$ molecules, and in contrast to the case of water clusters is not preceded by well-bound surface states for smaller clusters.[28] The critical sizes for electron binding to water and ammonia clusters are in agreement with experimental observations.[1-6]

(3) The smallest water cluster which attaches an excess electron is the water dimer. The binding energy is estimated to be between 3 meV[17,24] and 25 meV,[24,29,30] depending on the nuclear configuration. At 20 K transitions between cluster configurations occur, characterized by low and high molecular dipole moments, with corresponding low and high excess electron binding energies.[29,30]

(4) The mechanism underlying the mode of localization (surface vs. internal states) is a balance between the excess electron binding energy to the cluster and the energy associated with structural molecular reorganization in the cluster upon electron attachment. In the small- and medium-size water cluster regime ($n < 64$), the cluster reorganization energy associated with the formation of an internal electron state is large compared to that which is gained via binding, resulting in surface localization of the excess electron. The transition to internal localization is associated with a reversal of the balance between binding and reorganization energies.

(5) Studies[32] of the dynamics of excess electron migration, localization, and solvation, starting from an electron attached to cold large ($n = 256$) and medium ($n = 64$) $(NH_3)_n$ and $(H_2O)_n$ clusters in diffuse weakly bound surface states, show that the time scale for electron penetration into the cluster and the formation of an excess electron state exhibiting properties of an internally solvated electron is of the order of a few picoseconds ($\leqq 2$ ps for $(H_2O)_{256}^-$ and ~ 5 ps for $(NH_3)_{64}^-$ and $(NH_3)_{256}^-$). Thus, measurements on such negatively charged molecular clusters should yield similar results, regardless of the method of preparation (i.e., electron localization during the cluster nucleation process[1,3,4,6] or via capture of very low energy electrons by preexisting clusters[2,5]), provided that probing occurs past the short time required for penetration. The migration of the excess electron from the surface toward the middle of the cluster is characterized by a non-hopping, polaron-like, mechanism.[32]

(6) The vertical binding energies calculated via the QUPID simulations[23-27] for surface states of $(H_2O)_n^-$ clusters in the range $12 \leqq n \leqq 18$ are in good agreement with those available from photoelectron spectroscopy experiments.[6]

(7) From analysis of QUPID simulation results,[26,31] we conclude that the spectra of surface excess electron states in small- and medium-sized $(H_2O)_n^-$ ($8 \leqq n \leqq 32$) clusters are characterized by bound–continuum transitions and that the spectra of the energetically stable interior excess electron states in large $(H_2O)_n^-$ ($n \geqq 64$) clusters are characterized by bound–bound transitions.

(8) TDSCF simulations[30] show that the electronic absorption spectrum in $(H_2O)_n^-$ ($n \geqq 64$) clusters, which is primarily associated with overlapping transition from (s-like) ground state to the three (p-like) lowest excited states, is only slightly sensitive to cluster size. The calculated absorption peak predicted by these simulations is at ~ 2.1 eV and has a width of ~ 1 eV, compared to the experimental results[43] for bulk water of 1.72 eV and 0.92 eV, respectively.

(9) The relaxation dynamics following an electronic transition of an internally localized excess electron in water clusters at 300 K, investigated[33] using an adiabatic simulation method, is characterized by two time scales: (i) a very fast (20–30 fs) one associated with molecular rotations in the first solvation shell about the electron and (ii) a slower stage (~ 200 fs) which is of the same order as the longitudinal dielectric relaxation time in water. These time scales are not strongly sensitive to the cluster size ($n \gtrsim 60$) for $(H_2O)_n^-$ clusters which support internally bound ground and excited electronic states.

In this paper, we focus on issues related to dynamical processes and spectra of electrons in polar molecular

clusters. A description of the quantum simulation methods is given in Section 2. In Section 3 we review our recent studies of the dynamics of electron migration and solvation in water clusters. A discussion of the relaxation dynamics in negatively charged water clusters, following an electronic transition of the solvated electron, is presented in Section 4. The spectra of excess electrons internally localized in water clusters and the spectrum of an electron attached to a small ionic cluster (Na_2Cl and Na_2F) are discussed in Section 5.

2. SIMULATION METHODS

The time evolution of the wave function of a quantum particle moving in a potential $V(\mathbf{r})$ can be obtained via second-order differencing[36c] or by repeated applications of the split exponential time-evolution operator[36a,b,d] (for small time increments Δt) according to:

$$\begin{aligned}\psi(\mathbf{r}, t+\Delta t) &= \exp\left[-\frac{i}{\hbar}(\hat{K}+\hat{V})\Delta t\right]\psi(\mathbf{r}, t) \\ &= \exp\left[\frac{1}{2}\frac{i}{\hbar}\hat{K}\Delta t\right]\exp\left[-\frac{i}{\hbar}\hat{V}\Delta t\right] \\ &\quad\times\exp\left[-\frac{1}{2}\frac{i}{\hbar}\hat{K}\Delta t\right]\psi(\mathbf{r}, t) \\ &\quad + o((\Delta t)^3), \end{aligned} \tag{1}$$

where $\hat{K}$ and $\hat{V}$ are the kinetic- and potential-energy operators, respectively. An expansion in a plane-wave, free-particle, basis set yields:

$$\begin{aligned}\psi(\mathbf{r}, t+\Delta t) &= \frac{1}{(2\pi)^3}\exp\left[-\frac{i}{\hbar}\hat{K}\Delta t\right]\exp\left[-\frac{i}{\hbar}V(\mathbf{r})\Delta t\right] \\ &\quad\times\int d^3k e^{-i\mathbf{k}\cdot\mathbf{r}}\exp\left[-\frac{i\hbar k^2}{4m}\Delta t\right] \\ &\quad\times\int d^3r' e^{-i\mathbf{k}\cdot\mathbf{r}'}\psi(\mathbf{r}', t), \end{aligned} \tag{2}$$

where m is the mass of the quantum particle.

The Fourier transformations in the above equation are performed using the efficient FFT algorithm.[36d] Implementation of the FFT procedure requires that the wave function $\psi(\mathbf{r}, t)$ be defined on a grid, with periodic boundary conditions. We note that the grid representation, introduced in connection with the FFT, restricts the spatial resolution (determined by the mesh size) and the momentum (and thus the kinetic energy) range which can be described.[36] Thus, the size of the grid (i.e., the number of grid points) and its physical dimension must be appropriate for the physical system under study.

When the quantum subsystem interacts with a subsystem whose dynamical evolution can be described classically, a mixed quantum-classical time-dependent self-consistent set of equations can be derived[29,30,33,38,44] as a generalization of the TDSCF method,[36d,37] yielding:

$$\frac{\partial\psi(\mathbf{r}, \{\mathbf{R}_i\}, t)}{\partial t} = -\frac{i}{\hbar}\hat{H}(\mathbf{r}, \{\mathbf{R}_i\})\psi(\mathbf{r}, \{\mathbf{R}_i\}, t) \tag{3a}$$

$$\hat{H}(t) = \hat{K} + \hat{V}(\mathbf{r}, \{\mathbf{R}_i\}) \tag{3b}$$

and

$$M_j\ddot{\mathbf{R}}_j = \mathbf{F}_j - \nabla_{\mathbf{R}_j}U(\{\mathbf{R}_i\}) \tag{4a}$$

$$\begin{aligned}\mathbf{F}_j = &-\int d\mathbf{r}\psi(\mathbf{r}, \{\mathbf{R}_i\}, t) \\ &\times[\nabla_{\mathbf{R}_j}V(\mathbf{r}, \{\mathbf{R}_i\})]\psi(\mathbf{r}, \{\mathbf{R}_i\}, t),\end{aligned} \tag{4b}$$

where the integration is over the quantum particle coordinates. In the above equations, $\hat{H}(t)$ is the Hamiltonian of the quantum particle (with the implicit time dependence through $\{\mathbf{R}_i\}$). $\{\mathbf{R}_i\}$ denotes the collection of dynamical coordinates of the classical particles (with masses $\{M_i\}$, $i = 1, \ldots, N_c$), V is the interaction between the quantum and classical subsystems, and U is the interaction potential between the classical particles. $\mathbf{F}_j$ in Eqs. (4) is the self-consistent force acting on the classical particles, evaluated via the Hellmann–Feynmann theorem.

2.1. *The Adiabatic Simulation Method (ASM)*

While it is possible to implement the TDSCF formulation for studies of real-time dynamics of a quantum subsystem coupled to dynamical classical degrees of freedom, in most of the investigations described in this review we limit ourselves to the adiabatic time evolution of such a coupled quantum-classical system (i.e., an excess electron interacting with a classical polar cluster). This adiabatic simulation method[29,30,33] (ASM, and its ground-state dynamics, GSD, version) affords a significant reduction in computations time for processes which are essentially adiabatic as compared to the full real-time dynamical evolution. Clearly, the method is suited for situations where the subsystems comprising the system are characterized by widely separated time scales, such as the situations normally treated by the adiabatic or Born–Oppenheimer approximations. In fact, by construction the method is a numerical implementation of the adiabatic approximation where the electron (fast subsystem) is assumed (and is constrained) to remain at all times in a specified eigenstate of the Hamiltonian corresponding to the

instantaneous configuration of the classical particles (the slow subsystem).

The eigenstates of the Hamiltonian given in Eq. (3b) are the solutions of the Schrödinger equation:

$$\hat{H}(t)\,|\,\psi_l(\mathbf{r},\{\mathbf{R}_i(t)\})\rangle = E_l(t)\,|\,\psi_l(\mathbf{r},\{\mathbf{R}_i(t)\})\rangle, \quad l=0,1,2,\ldots . \tag{5}$$

The evolution of the classical subsystem on the potential energy surface corresponding to the lth state of the quantum subsystem is obtained via Eq. (4) with the wave function replaced by $\psi_l(\mathbf{r},\{\mathbf{R}_i(t)\})$. The desired state $|\,\psi_l(t)\rangle$ (where the electronic coordinate $\mathbf{r}$ and the explicit dependence on $\{\mathbf{R}_i\}$ have been dropped) can be obtained[45] from an arbitrary state $|\,\psi\rangle$ (assuming that the two are not orthogonal, i.e., $\langle\psi_l(t)\,|\,\psi\rangle \neq 0$) by the operation

$$\lim_{\beta\to\infty} e^{-\beta\hat{H}(t)}\hat{P}_l(t)\,|\,\psi\rangle \to \langle\psi_l(t)\,|\,\psi\rangle e^{-\beta E_l(t)}\,|\,\psi_l(t)\rangle, \tag{6}$$

where the projection operator, $\hat{P}_l(t)$, is given by

$$\hat{P}_l(t) = 1 - \sum_{m=0}^{l-1} |\,\psi_m(t)\rangle\langle\psi_m(t)\,|, \quad (l\neq 0), \tag{7}$$

and $\hat{P}_0(t)\equiv 1$ for the ground state ($l=0$, which is the case in GSD). As seen from Eq. (6), determination of an excited state l requires the prior determination of all the lower energy eigenstates. Note also that the operation in Eq. (6) can be regarded as evolution of the wave function in imaginary time $t=-i\beta$. This fact is conveniently used in converting the computer programs from performing real-time evolution of the wave function to the operation described by Eq. (6).

The above equations define the ASM. The numerical implementation of the operation on the left-hand side of Eq. (6) is achieved by the split-operator FFT method.[36] First, denoting $|\,\tilde{\psi}\rangle_l = \hat{P}_l(t)\,|\,\psi\rangle$, the left-hand side of Eq. (6) can be written as

$$e^{-\beta\hat{H}}\,|\,\tilde{\psi}\rangle_l = \lim_{J\to\infty}\prod_{j=1}^{J}(e^{-\beta\hat{K}/2J}e^{-\beta\hat{V}/J}e^{-\beta\hat{K}/2J})\,|\,\tilde{\psi}\rangle_l \tag{8}$$

Evaluation of the right-hand side of Eq. (8) proceeds by performing the $\hat{K}$ and $\hat{V}$ operations in the momentum and coordinate spaces, respectively (see Eqs. (1) and (2)). In these calculations, an error proportional to $\Delta\beta^3$, where $\Delta\beta=\beta/J$, is introduced due to the noncommutativity of the kinetic and potential energy operators. Also, in practical applications, the projection operation, Eq. (7), is performed several times during the imaginary time evolution, Eq. (8), in order to avoid the growth of lower state amplitudes due to numerical errors.

2.2. Application to Finite Systems

The introduction of the grid representation for the wave function and interaction potential between the quantum particle and the atoms ($V(\mathbf{r},\{\mathbf{R}_i\})$) implies a spatial periodicity of these quantities determined by the dimensions of the grid. In order to use the method for studies of finite systems (or in general for systems characterized by nonperiodic potentials) and, in particular, in studies of localized states, one must assure that the amplitude of the wave function under study, as well as the amplitudes of the wave functions corresponding to lower energy eigenvalues, vanish at the surface of the grid. These conditions can be satisfied for any localized state by simply assuring that the spatial extent of the employed grid is large enough. This can be accomplished either by increasing the number of grid points or by increasing the grid spacing. However, an increase in the number of grid points results in increased computation time, while increasing the grid spacing decreases the spatial resolution and, consequently, the energy range that can be accounted for.

In the problems which we discuss in this review, the excess electron density, $\rho(\mathbf{r})$, is localized, but its spatial extent and position may change in time. To facilitate the application of the FFT–GSD method to these systems, we have developed[32,33] an efficient "moving grid" algorithm in which the position and spatial extent of the density are monitored and the grid is adjusted accordingly, thus addressing the issues mentioned above. For details of the algorithm, the reader is referred to the original papers.[32,33]

2.3. The Electron–Molecule Pseudopotential

A key issue in modeling the system by the one-electron QUPID and TDSCF methods is the choice of interaction potentials. Fortunately, for small water clusters, interaction potential functions that provide a satisfactory description for a range of properties are available. We have used the RWK2-M model[39] for the intra- and inter-water interactions. Less is known about the electron–water interaction. We have constructed[23–25] a pseudopotential that consists of Coulomb, polarization, exclusion, and exchange contributions:

$$V(\mathbf{r}_e,\mathbf{R}_0,\mathbf{R}_1,\mathbf{R}_2) = V_{coul} + V_p + V_e + V_x. \tag{9a}$$

The positions of the oxygen and hydrogen nuclei of the water molecule are given by $(\mathbf{R}_0,\mathbf{R}_1,\mathbf{R}_2)$, and r_e is the position of the electron.

The Coulomb interaction is:

$$V_{coul}(\mathbf{r}_e,\mathbf{R}_0,\mathbf{R}_1,\mathbf{R}_2) = -\sum_{j=1}^{3} q_j e/\max(|\,\mathbf{r}_e-\mathbf{R}_j\,|,\mathbf{R}_\infty), \tag{9b}$$

where $\mathbf{R}_3 = \mathbf{R}_0 + (\mathbf{R}_1 + \mathbf{R}_2 - 2\mathbf{R}_0)\delta$ is the position of the negative point of charge of the RWK2-M model; q_1 and $q_2 = 0.6e$, $q_3 = -1.2e$, and $\delta = 0.2218756$. The values of q_j and δ were chosen[39] to give a good representation of the dipole and quadrupole moments of the water monomer. The cut-off radius, R_∞, was taken to be $0.5a_0$, and the results are insensitive to the precise value of R_∞.

The polarization interaction is given by

$$V_p(\mathbf{r}_e, \mathbf{R}_0) = -0.5\alpha e^2/(|r_e - R_0|^2 + R_p^2)^2, \quad (9c)$$

where $\alpha = 9.7446$ au is the spherical polarizability of the water molecule. The form of V_p and the value of $R_p = 1.6a_0$ were chosen to fit approximately the adiabatic polarization potential as calculated by Douglass et al.[46] for an approach of the electrons along the H–O–H bisector (see table 7 and fig. 2 in Ref. 46).

The exclusion, V_e, and the exchange, V_x, contributions both require the electron density $\rho(\mathbf{r}, \mathbf{R}_0, \mathbf{R}_1, \mathbf{R}_2)$ of the water molecule. We find that a reasonable fit to the calculated electron density[47] in the regions of importance is provided by:

$$\rho(\mathbf{r}, \mathbf{R}_0, \mathbf{R}_1, \mathbf{R}_2) = 8a_0^{-3}e^{-3|\mathbf{r}-\mathbf{R}_0|/a_0} + a_0^{-3}\sum_{j=1}^{2} e^{-3|\mathbf{r}-\mathbf{R}_j|/a_0}. \quad (9d)$$

The repulsion, due to the exclusion principle, is modeled as a "local kinetic energy term."[48] This contribution accounts for the orthogonality constraint between the wave function of the excess electron and the valence molecular electronic orbitals. In our calculation, this contribution is modeled as

$$V_e(\mathbf{r}_e, \mathbf{R}_0, \mathbf{R}_1, \mathbf{R}_2) = 0.5e^2a_0(3\pi^2\rho)^{2/3}. \quad (9e)$$

Finally, the exchange contribution, which is a consequence of the antisymmetrization of the wave function, is modeled within the local exchange approximation[49] by

$$V_x(\mathbf{r}_e, \mathbf{R}_0, \mathbf{R}_1, \mathbf{R}_2) = -\alpha_x e^2(3\pi^2\rho)^{1/3}/\pi. \quad (9f)$$

The parameter α_x was taken to be $\alpha_x = 0.3$ in order to obtain good agreement between our simulation results and the SCF results of Rao and Kestner[11b] for $(H_2O)_8^-$ at a fixed octahedral configuration of the water molecule.

3. DYNAMICS OF ELECTRON MIGRATION AND SOLVATION IN POLAR MOLECULAR CLUSTERS[32]

The mechanisms and dynamics of electron solvation and migration in fluids are key issues in advancing our understanding of a number of important chemical and physical phenomena such as carrier mobility, electron transfer reactions,[50] electrochemical processes and chemical reactions in solution,[51] electron solvation in fluids,[18,38,52–55] and electron attachment and localization in clusters.[19,20,32,33]

The main issues concerning the dynamics of excess electrons in polar fluids are the mechanisms of localization, trapping, and solvation and the spectroscopic consequences of these processes.[32,33,38,53–55] With regard to the initial stage of localization of an excess electron in polar fluids, contributions due to both preexisting trapping sites[53–60] as well as charge-induced polarization[61–63] have been considered. Considerable experimental and theoretical evidence has been advanced that both processes may contribute. Most recently it was concluded from theoretical investigations,[58] based on calculations of excess electron states for representative solvent configurations generated via classical molecular dynamics at 283 K, that upon the introduction of an excess electron into pure liquid water and prior to any induced liquid configurational relaxation, the electron can be physically localized in a distribution of shallow ground states, and that under these circumstances localized excited states are rare. Moreover, recent experiments[53] in which the time evolution of the optical absorption spectrum of excess electrons in water was studied at the femtosecond time scale have shown an initial rise of a broad infrared (IR) absorption with a characteristic time scale of $\lesssim 110$ fs, which can be assigned as originating from shallow initial ground-state trapping or from an excited state of the excess electron. Following this stage, a coincident disappearance of the initial state and a relaxation into the fully solvated state were observed with a characteristic time scale of 240 fs. Furthermore, the absence of spectral shift during the time evolution between these two stages of solvation had been noted, and it was tentatively suggested[53] that the second stage may correspond to an electronic transition, perhaps mediated by the dieletric relaxation of the medium.

In our studies, we focus on the dynamics of excess electrons in finite polar molecular clusters ($(NH_3)_{256}^-$ and $(H_2O)_{256}^-$; in the following, we present results for the water cluster). These systems introduce new aspects in relation to studies of excess electron in bulk fluid systems, such as the inherent inhomogeneity of the system (i.e., surface and interior cluster environments), the distinction between surface and interior modes of electron localization,[19,20,24–31] and the process of penetration[32] (when the internal localization mode is thermodynamically favorable). Nevertheless, it is worthwhile to note that the separation of dynamical stages which we find for these systems (particularly the

sudden transition from a shallow bound state to an almost fully solvated state and the corresponding sudden change in the excitation spectrum) and the time scales on which they occur are reminiscent of the temporal stages and their spectral manifestations discussed in the context of time-resolved spectroscopy of electron localization and solvation in bulk fluids.[53]

3.1. Temporal Evolution

We start our simulation with a phase-space configuration of the neutral molecular cluster (nuclear positions and momenta) selected at random from the canonical equilibrium ensemble at the desired temperature (300 K for $(H_2O)_{256}^-$). Using the FFT method, the ground state of an excess electron attached to the selected neutral cluster configuration (with the nuclear positions kept frozen) is obtained. The so obtained initial ground state is characterized by a diffuse excess electron density distribution with low binding energy (-0.008 Hartree for $(H_2O)_{256}^-$, for the particular initial configurations used in the present simulations). Having prepared the initial state in this manner, the nuclear coordinates are allowed to evolve in time (starting with the initial selected velocites) and the excess electron ground-state wave function corresponding to the instantaneous nuclear coordinates is reevaluated after each integration time step of the equations of motion of the nuclear coordinates. Throughout the simulations, the total energy of the system remains constant.

The time evolution of the excess electron ground-state energy (E_0) and of its kinetic (K) and potential (V) components is shown in Fig. 1a, and the distance of the center of the excess electron density ($\mathbf{r}_e$) from the molecular cluster center of mass (r_{cm}) and the width $r_g = \langle\psi_0|(\mathbf{r}-\mathbf{r}_e)^2|\psi_0\rangle^{1/2}$ of the ground-state electron density distribution are shown in Fig. 1b. In addition, we show in Fig. 1a the values of the first three excited states, at selected times during the evolution (denoted by dots). Four temporal stages of the evolution of the systems can be discerned from these figures.

Stage 1: $t = 0$–0.15 ps. This stage is characterized mainly by the initial reorganization of the cluster in response to the presence of the electron, exhibited by reorientation of the molecules resulting in a decrease in magnitude of the intermolecular interaction potential energy and an increase in the dipole moment of the cluster. Coupled to the cluster reorganization are an increase in the magnitude of E_0 (from -0.008 Hartree at $t = 0$ to -0.03 Hartree at 0.15 ps), a decrease in the width of the wave function (see $r_g = \langle\psi_0|(\mathbf{r}-\mathbf{r}_e)^2|\psi_0\rangle^{1/2}$ in Fig. 1b), and an increase in the separation between

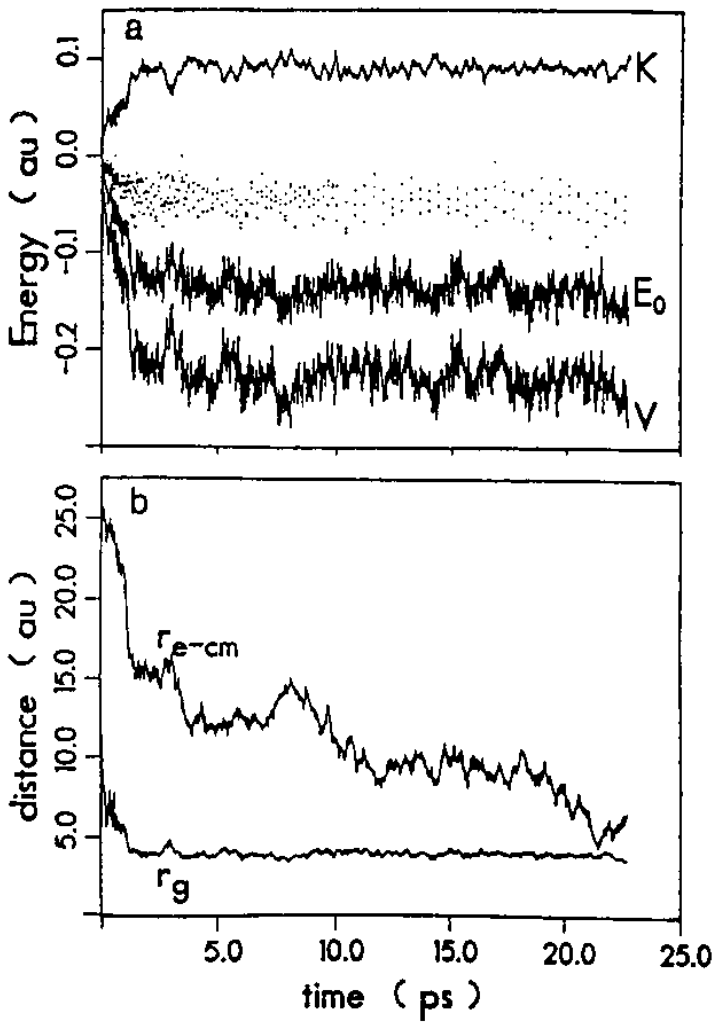

Fig. 1. Time evolution of an excess electron in a $(H_2O)_{256}^-$ cluster at $T = 300$ K. a. The electron ground-state energy, E_0, and the potential, V, and kinetic, K, energy contributions for $0 \leqq t \leqq 23.0$ ps. The first three excited states are given at selected times by the dots. b. Width of the electron distribution, r_g, and distance of the center of the excess electron distribution from the cluster center of mass, $r_{e\text{-}cm}$, vs. time. Energies and distances in atomic units (Hartree and Bohr radius) and time in picoseconds.

the electronic ground state and first excited states ($\Delta E_1 = E_1 - E_0$; see Fig. 1a). Thus, while at the beginning of the simulations the conditions under which the GSD method is valid (i.e., the adiabatic approximation) are not fully satisfied, towards the end of stage 1 the use of the GSD method is fully justified. This conclusion was substantiated by comparing, at various stages of the dynamical evolution, the results obtained via GSD with those obtained by following the *real-time evolution*, without the ground-state constraint, within the TDSCF approximation.

Stage 2: 0.15 ps $\leqq t \leqq$ 1.2 ps. During this stage, the excess electron remains bound in a surface state and explores various sites on the surface of the cluster. The

motion of the electron is accompanied by a significant increase in the magnitude of E_0, a gradual variation in the excitation spectrum (shown in Fig. 2), and a significant reorganization of the molecular cluster, mainly in the vicinity of the electron, evidenced by the further increase of the intermolecular potential energy and of the magnitude of the cluster dipole moment. We note that the increase in the intermolecular potential energy is approximately equal to the increase in magnitude of the excess electron energy, E_0, while the intramolecular potential energy and the kinetic energy of the atomic constituents are fluctuating about a constant value.

While during this stage the electron is confined mainly to the outer region of the cluster, the initial stage of the electron solvation process begins as evidenced by an increase in the number of near neighbor molecules (see Fig. 3a). In this figure, the number of molecules in a sphere of radius $10a_0$ centered on $\mathbf{r}_e$ (shell s1) and a decomposition into subshells (0–$7.0a_0$ (s1a) and $7.0a_0$–$10a_0$ (s1b)) are shown (the choice of these shell radii is guided by the radial distribution of the molecules around the fully solvated electron, see below). As seen, the major increase in the number of neighboring molecules is in the outer range of $7.5a_0$–$10a_0$ (shell s1b in Fig. 3a).

In addition to the radial distribution of molecules, the local environment of the electron can be characterized by the orientation of the molecules with respect to the center, $\mathbf{r}_e$, of the excess electron density. In Fig. 3b,c plots of $\langle\cos(\theta_{\text{bond}})\rangle$ and $\langle\cos(\theta_{\text{dipole}})\rangle$ are shown for molecules in shells s1a and s1b, where

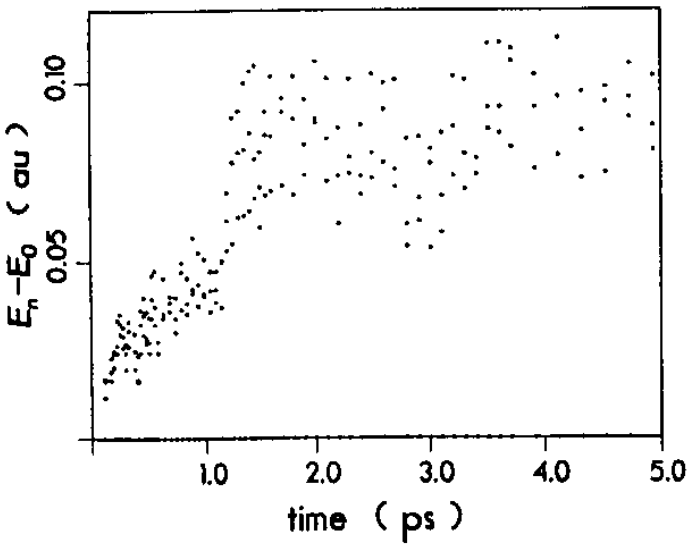

Fig. 2. The excitation spectrum, $E_n - E_0$, $n = 1$–3, of an excess electron in $(H_2O)_{256}^-$ for $0 \leqq t \leqq 5$ ps. No significant variation occurs beyond the time span shown. Note the sharp increase in the excitation spectrum at $t \approx 1.2$ ps.

$$\cos(\theta_{\text{bond}}) = \max\left[\frac{(\mathbf{r}_e - \mathbf{r}_0)\cdot(\mathbf{r}_H - \mathbf{r}_0)}{|\mathbf{r}_e - \mathbf{r}_0|\,|\mathbf{r}_H - \mathbf{r}_0|}\right], \tag{10a}$$

and

$$\cos(\theta_{\text{dipole}}) = \frac{(\mathbf{r}_e - \mathbf{r}_0)\cdot\boldsymbol{\mu}}{|\mathbf{r}_e - \mathbf{r}_0|\,|\boldsymbol{\mu}|}, \tag{10b}$$

where $\mathbf{r}_0$ is the location of the oxygen atom in a water molecule and $\mathbf{r}_H$ is the location of that hydrogen atom of the molecule whose O–H bond forms the minimum angle with respect to $\mathbf{r}_e - \mathbf{r}_0$. $\boldsymbol{\mu}$ is the dipole moment of the molecule, and the angular brackets indicate averages over the molecules within the radial shells. For a random distribution of the molecular orientations in water, $\langle\cos(\theta_{\text{bond}})\rangle = 0.3954$. From Fig. 3b,c we observe that following the increase in both $\langle\cos(\theta_{\text{bond}})\rangle$ and $\langle\cos(\theta_{\text{dipole}})\rangle$ in Stage 1, they fluctuate about values which correspond to a high degree of bond orientation (i.e., O–H bonds pointing to the center of the excess electron density) for molecules within $7.0a_0$–$7.5a_0$ from the electron as well as to preferred dipole orientation for the neighboring molecules. This ordering is considerable also in the second subshell (s1b, see Fig. 3c). To investigate the spatial range over which orientational ordering occurs, the number of molecules in more distant shells ($10a_0$–$15a_0$, s2; and $15a_0$–$25a_0$, s3) as well as $\langle\cos(\theta_{\text{dipole}})\rangle$ and the interaction potential between the excess electron and the molecules are given in Fig. 4. The dipole orientation parameter, $\langle\cos(\theta_{\text{dipole}})\rangle$, for the more distant shells shown in Fig. 4b indicates less pronounced orientational ordering than in the vicinity of the electron (shell s1), which correlates with the smaller values of the interaction energy between molecules in these shells and the excess electron (see Fig. 4c). Nevertheless, the long-range nature of the interaction should be noted.

Stage 3: 1.2 ps $\leqq t \leqq$ 1.5 ps. Following the formation of a well-bound surface state during Stage 2, the system evolves in a dramatic manner signified by sharp changes in energetic and structural characteristic quantities. In this stage, the first molecular solvation shell around the excess electron is completed. As seen in Fig. 3a, the number of molecules within $7.0a_0$ or $7.5a_0$ from $\mathbf{r}_e$ (subshell s1a) increases suddenly to about six (at ~ 1.25 ps) and fluctuates about this value for the remainder of the simulation. In conjunction with the formation of the solvation cavity, the excess electron density contracts (see r_g in Fig. 1b) and the center of density penetrates towards the center of the cluster (see $r_{e\text{–}cm}$). Note also that the formation of the first solvation shell results in a decrease in the orientational order of

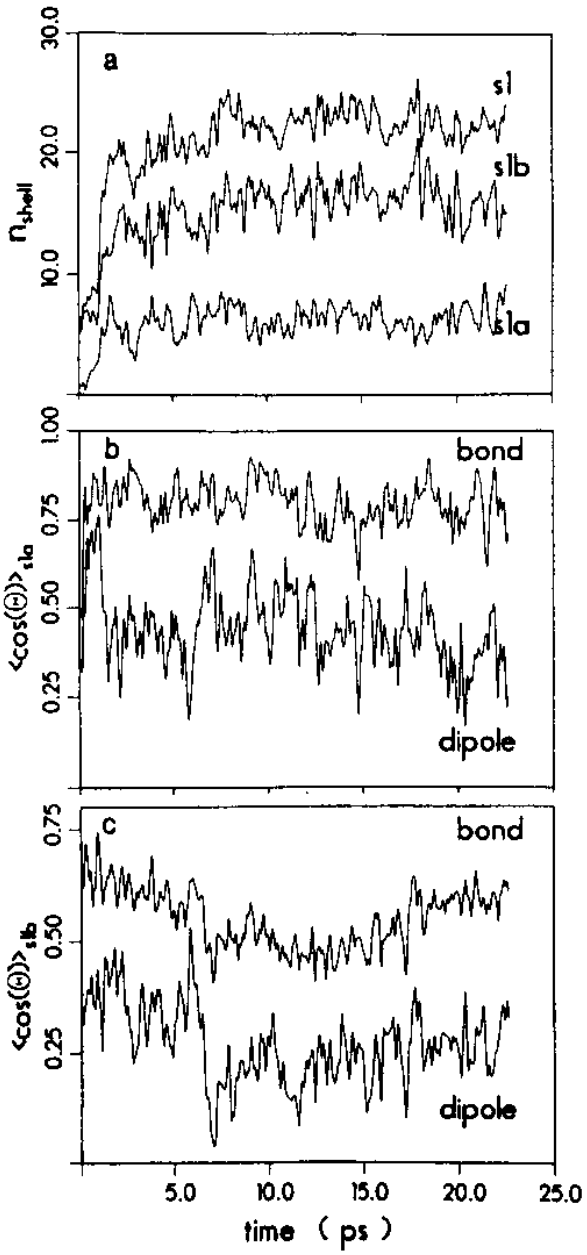

Fig. 3. a. The number of water molecules, n, vs. time in the first shell (s1) around the center of the excess electron density, r_e. Shell s1 is defined in the range $(0, 10a_0)$; subshells s1a and s1b in the intervals $(0, 7.0a_0)$ and $(7.0a_0, 10a_0)$, respectively. The choice of shells is guided by the molecular distribution about the fully solvated electron. b,c. Time variation of the cosine of the angle between $\mathbf{r}_e - \mathbf{r}_0$ and the water molecular dipoles and between $\mathbf{r}_e - \mathbf{r}_0$ and the bond vector $\mathbf{r}_H - \mathbf{r}_0$ forming the minimum angle with respect to the former vector in subshells s1a and s1b. For a random distribution of the molecular orientations, $\langle\cos(\theta_{bond})\rangle = 0.3854$ and $\langle\cos(\theta_{dipole})\rangle = 0$.

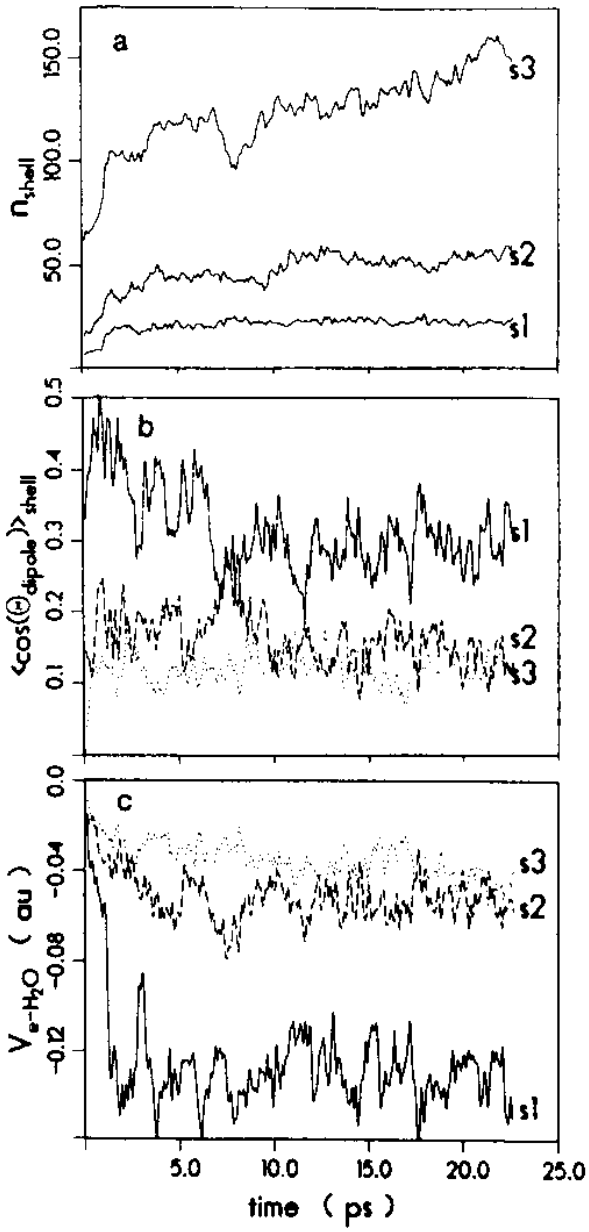

Fig. 4. a. The number of water molecules, n, vs. time in shells around $\mathbf{r}_e$: s1 $(0, 10a_0)$; s2 $(10a_0, 15a_0)$; s3 $(15a_0, 25a_0)$. b. Same as Fig. 3b for the above shells. c. Excess electron–water interaction potential energy decomposed into shells.

more distant molecules and a decrease in the total cluster dipole moment due to screening of the excess electron charge by the first solvation shell.

These structural changes are accompanied by pronounced sudden changes in the excess electron ground-state potential and kinetic energies (Fig. 1a) and excitation energies (see Fig. 2). Note that these changes occur in less than 1 ps and correlate with the sudden increase in the number of molecules within $7.0a_0$ of $\mathbf{r}_e$. The values of the electron ground-state energy, E_0, and excitation energies at the end of this fast stage are close to those of the fully solvated electron. In this context, we note that the calculated sudden increase in the excitation energies, which would exhibit itself as a shift of the absorption spectrum to shorter wavelength, is reminiscent of the shift in the absorption spectrum from an initial absorption peaking in the IR to an absorption maximum at the wavelength characteristic of the fully solvated electron observed in recent studies of the dynamics of excess electron solvation in liquid

water following photoionization[53] and in theoretical studies of electron solvation.[38,58]

Stage 4: $t > 1.5$ ps. Having established in Stage 3 a local environment characteristic of a fully solvated electron, the systems continue to evolve with the migration of the excess electron towards the center of the cluster accompanied by a gradual buildup of successive solvation shells (see Fig. 4a,c). Radial distribution functions of the molecular oxygens and hydrogens about the electron center of density, towards the end of the simulations, are shown in Fig. 5 for $(H_2O)_{256}^-$ at two temperatures.

Further information about the structure and energetics of the fully solvated electron in $(H_2O)_{256}^-$ is obtained from a radial plot of the excess electron potential energy shown in Fig. 6 for two temperatures. In this figure as well as in the atomic radial distribution functions, the formation of a clearly defined solvation shell structure is evident. As seen, the effect of higher temperature is to somewhat blur the distinction of solvation shells beyond the first one.

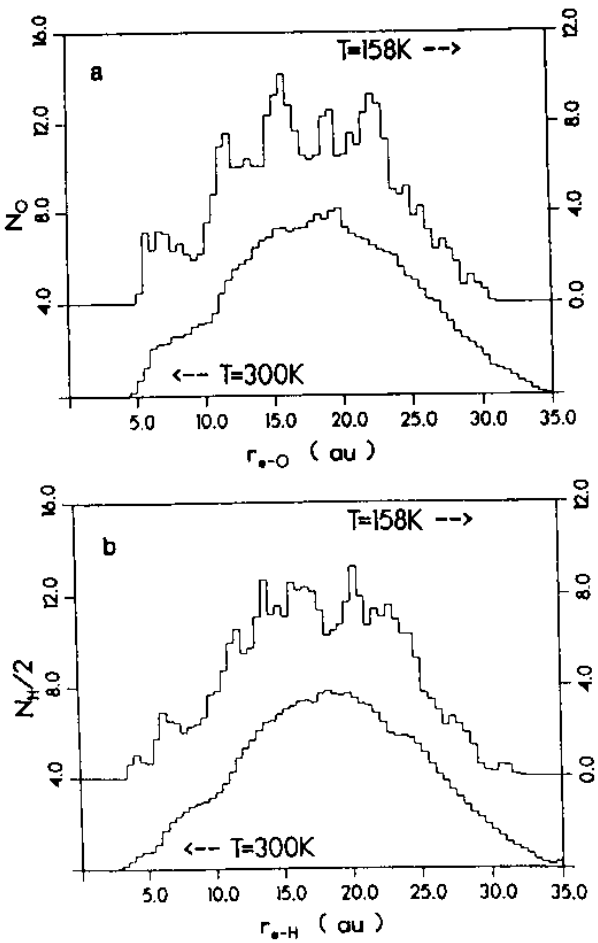

Fig. 5. Radial distribution of oxygens (a) and hydrogens (b) about the center of the excess electron density in the fully solvated state in $(H_2O)_{256}^-$, at $T = 158$ K and 300 K.

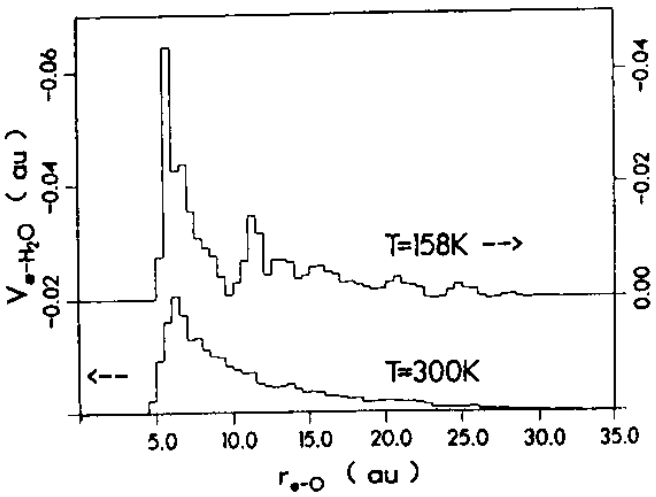

Fig. 6. Radial distribution of the excess electron–molecule interaction potential energy in $(H_2O)_{256}^-$, in the fully solvated state, at $T = 158$ K and 300 K. Note the marked solvation shell structure and the blurring of that structure beyond the first shell at the higher temperature.

Finally, we note that the solvation shell strucure and the tendency of molecules in the first solvation shell to be bond-oriented, rather than dipole-oriented, towards the center of the excess electron distribution found in these simulations (as well as in our previous QUPID simulations of excess electrons internal localization in water[26] and ammonia[28] clusters) are in agreement with results obtained via simulations[42] of electron hydration in bulk water in which a different interaction potential for the interaction between water molecules, as well as between the excess electron and the molecules, was used. Furthermore, bond orientation is exhibited in our simulations already at the initial stages of the electron penetration process, even before the first solvation shell is completely developed. This observation indicates the role of local orientational reorganization of the molecules, in the vicinity of the excess electron, in the process of localization (trapping) of the initial surface state.

3.2. *Mode of Electron Migration*

In the above we have investigated the time evolution of the coupled electron–cluster system and have exhibited the structural and energetic temporal variations in the properties of the system as the electron solvates in an internally localized state. We turn next to a discussion of the nature of the electron penetration (migration) process. This process clearly involves quantum-mechanical evolution of the electron coupled to the dynamics of the cluster environment. In fact, the molecular reorganization of the molecular cluster is essential for the evolution of the solvated state which

does not develop if the classical degrees of freedom of the cluster are frozen in their initial state configuration.

In studying the migration of an electron in condensed media which do not possess translational periodicity (i.e., in our case, the penetration of the electron from the external surface to the interior of the cluster), several modes of propagation may be considered. Studies of excess electron migration in molten salts[44a] suggest that the electron transport in these systems is mostly due to short-time jumps between two spatially separated sites. This mechanism is characterized by the occurrence of configurations where at the intermediate time (between sites) the wave function exhibits splitting (i.e., a bimodal electron density distribution is found), and it appears that a potential barrier separates the initial and final localized states of the electron.[44a] In our simulations we did not find evidence for such electron hopping events. In particular, we did not find configurations of the excess electron which are characterized by a bimodal distribution of the electron density distribution. Such events would have been exhibited in large variations in the width of the excess electron distribution, r_g, which are absent in our results (see Fig. 1). We remark that the fact that the excess electron wave function remains localized at all times serves as a posterior consistency check on the employment of the TDSCF method in our simulations.

Monitoring of the structural and energetic properties of the system reveals that the propagation of the electron in the cluster is accompanied by structural reorganization of the cluster environment in the vicinity of the solvated electron and that the migration of the electron into a specified region is accompanied by an increase in the number of molecules in that region. For molecules in the first solvation shell (s1a ($0–7a_0$)), the reorganization energy per molecule is of the order of a hydrogen bond energy in water.

The difference between the electron migration mechanisms in molten alkali halides[44a] and in our polar molecular systems may be attributed to the difference in the host reorganization energy in these systems. In the case of molten alkali halides, the solvated electron substitutes for a halide anion and the energy of the region containing the electron is close to that of neighboring regions in the fluid. On the other hand, in a polar molecular system the energy of a region around the solvated excess electron is much larger in magnitude than that of an equivalent neighboring neutral region. Furthermore, in the latter case, due to the sizeable reorganization energy[26] which accompanies the formation of the solvation shells, solvent fluctuations leading to a favorable solvation site in a neutral region are unlikely. Indeed, the absence of deep traps in neutral water has been recently demonstrated.[58]

As shown by our previous QUPID calculations,[23–28] the adiabatic binding energy (i.e., the electron ground-state energy plus the cluster reorganization energy) of an excess electron to a polar molecular cluster favors internal localization for sufficiently large clusters ($n \gtrsim 64$ for $(H_2O)_n^-$ and $n \gtrsim 32$ for $(NH_3)_n^-$). In addition, a continuum dielectric model for excess electrons in finite molecular aggregates[26,27] yielded results in agreement with these calculations and experimental data and demonstrated the importance of the long-range polarization interaction in stabilizing the solvated state. As seen from Fig. 4c, while the largest contribution to the electron potential energy comes from its interaction with the first solvation subshell, s1a ($0–7.0a_0$ for water and $0–7.5a_0$ for ammonia), which is fully developed at an early stage, the long-range interaction with the furthest away molecular shells and the development of these shells provide the driving force for migration from the surface to the interior where that contribution is maximized. The mechanism of migration is polaron-like in nature, with the electron propagating in a spatially localized solvated ground state via polarization of the dynamical host environment (no "dragging" of molecules accompanies the migration of the electron). The spectral consequences (i.e., the sudden increase in the excitation energy, see Fig. 2) of the time evolution of the electron–cluster system remain an experimental challenge.

Finally, we note that the time scale for electron penetration from the surface into the cluster and the formation of an excess electron state exhibiting properties of an internally solvated electron are of the order of a few picoseconds (< 2 ps for $(H_2O)_{256}^-$ at 300 K and ~ 5 ps for $(NH_3)_{64}^-$ and $(NH_3)_{256}^-$ at 189 K). From this observation we conclude that both methods of preparation of such negatively charged molecular clusters (i.e., electron localization during the cluster nucleation process[1,3,4,6] or via capture of very low energy electrons by preexisting clusters[2,5]) would yield similar results, as long as probing of the clusters occurs past the short time required for penetration.

4. RELAXATION DYNAMICS FOLLOWING TRANSITIONS OF SOLVATED ELECTRONS

The dynamics of polar solvent reorganization associated with changes in the charge distribution of a solute species has been an active area of research in the last two decades.[64–66] Such studies deal with the dynamics of solvent relaxation associated with molecular excitation,[67–76] ionic solvation,[77–79] electron

transfer,[80-88] and electron localization[53,54,89-93] in polar solvents. Theoretical studies of these phenomena have usually invoked a continuum dielectric model for the solvent, specified by its dielectric dispersion $\varepsilon(\omega)$.[77,94-104] More recently, several studies where the molecular nature of the solvent was accounted for in an approximate manner have been published.[63,105-110] In particular, a combination of linear response theory with the dynamical mean spherical approximation (MSA), originally developed by Wolynes[108] and later further developed and applied by Rips et al.[109] and by Nichols and Calef,[110] was recently shown by Maroncelli and Fleming[111] to account well for the main trends in the experimental molecular fluorescence results.

An alternative approach to the dynamics of solvation phenomena is provided by numerical simulations, and several such studies have been published for aqueous solutions.[38,78,79,112,113] Such studies, in particular the very detailed one by Maroncelli and Fleming,[79] have provided much insight into the molecular nature of the solvation process. Their relevance to the actual experimental systems depends, of course, on the quality of the potential used. It should be pointed out that such simulations of aqueous solutions are of particular importance because the validity of simple models such as the MSA[77] is questionable for such a highly associated and highly structured solvent.

Technological advances in the creation and detection of ultrashort optical signals have made it now possible to follow solvation dynamics in such systems where the longitudinal dielectric relaxation time τ_L is $\lesssim 0.5$ ps. In particular, Migus et al.[53] have followed the subpicosecond evolution of the electron absorption spectrum following electron injection (by photoionization) in bulk water (following the ~ 100-fs ionization pulse) where absorption in the near IR, which seems to build up with a characteristic time of ~ 110 fs, and a subsequent decay of this signal and a buildup of absorption in the $\lambda = 700$–900-nm region on a time scale of ~ 240 fs were observed.

Most recently, Rossky and co-workers[38,114] have performed simulations of this system employing the simple point charge (SPC) water potential model and a pseudopotential for the electron–water interaction. The starting points of these simulations are ground states of the electron calculated for static water configurations selected from an equilibrium ensemble obtained in the absence of the electron. Analysis of the energy distribution associated with the ground and excited electronic states obtained for these neutral water configurations yields an absorption lineshape which is consistent with the experimentally observed initial IR absorption. Based on their results, Rossky and Schnitker[38] have concluded that the GSD simulation is not adequate for the early stages of electron solvation in water and that the first species observed after the ionizing pulse in the Migus et al. experiment[53] is a solvated excited state. They propose that the rate-determining step in the subsequent evolution towards the fully hydrated electron in its ground state is the nonadiabatic transition from the excited to the ground state.

In order to gain further insight into the relaxation processes associated with the solvated electron and into the solvation process, we have performed adiabatic simulations of negatively charged water clusters following transitions of the excess electron between the ground electronic state and the lowest excited electronic state.[33] We have simulated the cluster relaxation following a transition from the ground to the excited electronic state, as well as following the reverse electronic transition, i.e., a deexcitation from the excited to the ground state. Most relevant to the results discussed above is the second relaxation process; however, we find that both of them behave quite similarly. In both cases, the relaxation is seen to proceed in a nonexponential fashion with at least two times scales involved: a fast one (~ 20–30 fs for room temperature clusters), during which the energy gap between the two electronic states changes to about 60% of its final value and the width of the electron wave function (the electron "radius of gyration") relaxes to approximately its final value, and a relatively slow (~ 250 fs) time scale during which the electronic energy gap becomes fully developed. These time scales are not strongly sensitive to the cluster size for $(H_2O)_n^-$ clusters which support internally bound ground and excited electronic states ($n \gtrsim 60$; actual simulations were done with $n = 64$ and $n = 128$). They are, however, strongly sensitive to deuterium isotope substitution and also depend on the cluster temperature.

The adiabatic simulation method employed in our studies, where the electron is restricted to stay in one electronic state which evolves adiabatically with the nuclear configuration, as well as the interaction potentials, were described in Section 2. It should be pointed out that restricting the excited state evolution to the lowest electronic state is somewhat artificial: the energies of the three lowest p-like excited states are not far apart (thus, while the average energy spacings between these states in the $(H_2O)_{128}^-$ are from our simulations ~ 0.3 eV, these energies fluctuate with the cluster configurations and can become close to each other: we have observed typically one–two near crossing events, $\Delta E \lesssim kT$ for $T = 300$ K, between the first and second

excited state in 1-ps trajectories), so that nonadiabatic transitions between them cannot be ruled out. However, such occurrences are rare on the simulation time scales discussed below and should not have an appreciable effect on the observed solvation dynamics.

The main technical details of the simulations are as follows: a time step of 10 au ($= 2.4 \times 10^{-16}$ s) is used for the classical particles using the velocity version of the Verlet algorithm. The grid used for the electronic wave functions of the $(H_2O)_{64}^-$ cluster consists of 32^3 points with grid spacing $a = 1.2$ au, and for the $(H_2O)_{128}^-$ cluster, a 16^3 grid is used with $a = 1.5$ au. The need for a larger grid for the $(H_2O)_{64}^-$ cluster arises because the excited state wave function is relatively extended and is not described well on the smaller grid for this cluster size. The imaginary time step for the electronic state relaxation was taken to be 0.6 au. Finally, our simulations are performed at constant temperature (canonical ensemble) via employment of the stochastic collision method where at each integration time step of the classical subsystem the velocities of randomly selected atoms are thermalized according to a Maxwell–Boltzmann velocity distribution corresponding to the desired temperature. We have also run a few constant energy trajectories obtaining similar results.

Using this procedure, we have generated nuclear trajectories for motion either on the ground or on the excited potential surface. The wave functions and the electronic energies associated with both electronic states are calculated along these trajectories, yielding the adiabatic evolutions of these quantities as well as of related quantities such as the electronic vertical energy gap, the transition dipole moment between the two electronic states, and the electron gyration radius.

The calculations described below are aimed at elucidating the details of the time evolution of the nuclear configurations following a sudden switching from the ground to an excited electronic state or from the excited to the ground electronic state. To this end we have selected several equilibrium configurations of the $(H_2O)_{64}^-$ and the $(H_2O)_{128}^-$ clusters in the ground electronic state and followed the time evolution of the nuclear configuration and the associated electronic energies after switching, at time $t = 0$, from the ground to the excited electronic state. Thus, starting from a ground state configuration, the water molecules begin their motion on the (lowest) excited electronic potential surface, and the subsequent evolutions of both the classical (water) and quantum (electron) subsystems are followed. Subsequently, after full relaxation of the system on the excited state potential surface has been achieved, the electronic state is switched back to the ground state, and the subsequent relaxation to the ground state configuration is observed. Since our results demonstrated only a weak dependence on cluster size, we show mainly results obtained for the $(H_2O)_{128}^-$ cluster.

Figure 7 depicts the time evolution of the ground (E_0) and first excited (E_1) electronic energies of the $(H_2O)_{128}^-$ cluster, following a sudden switch from the ground to the first excited state. Figure 8 shows the corresponding evolutions of the energy gap, $\Delta E = E_1 - E_0$. The time-dependent widths (gyration radia, $(\langle r^2 \rangle - \langle r \rangle^2)^{1/2}$, where the expectation value is taken over the excess electron wave functions) of the ground and excited electronic state configurations for $(H_2O)_{128}^-$ are depicted in Fig. 9. The time evolution of the transition dipole

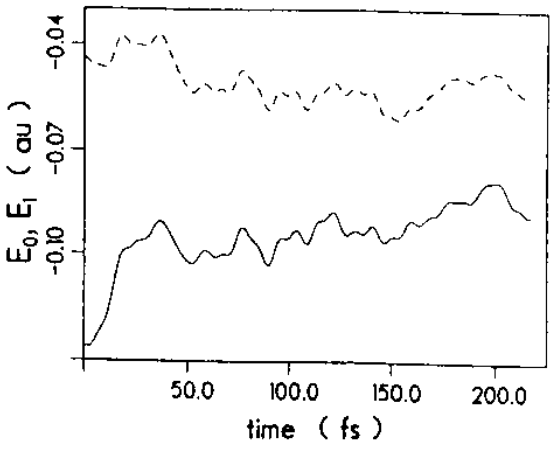

Fig. 7. Time evolution of the ground (E_0, full line) and of the first excited (E_1, dashed line) state energies of the solvated electron in $(H_2O)_{128}^-$ following a sudden excitation (at $t = 0$) from the ground to the first excited state. The results, as well as those shown in Figs. 8–10, are averaged over five runs in each case.

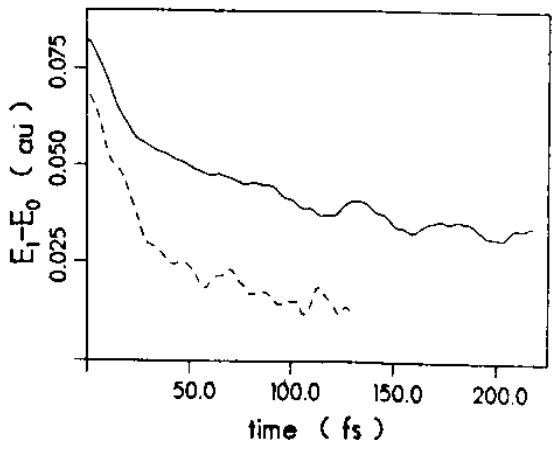

Fig. 8. Time evolution of the energy gap $\Delta E = E_1 - E_0$ for $(H_2O)_{64}^-$ (dashed line) and $(H_2O)_{128}^-$ (full line) following a sudden excitation (at $t = 0$) from the ground to the first excited state.

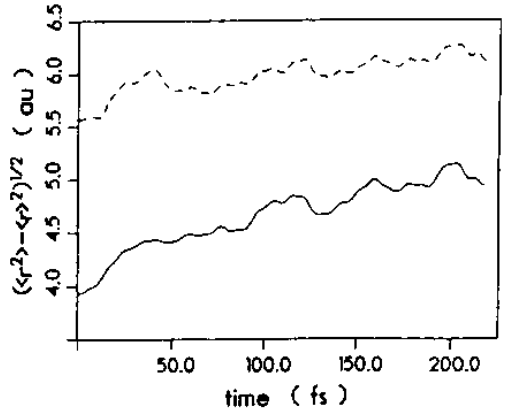

Fig. 9. Time evolution of the electron gyration radius, $((r^2) - (r)^2)^{1/2}$ following a $t = 0$ transition from the ground to the first excited state in $(H_2O)_{128}^-$. Full line = radius of the ground electronic state; dashed line = radius of the excited state.

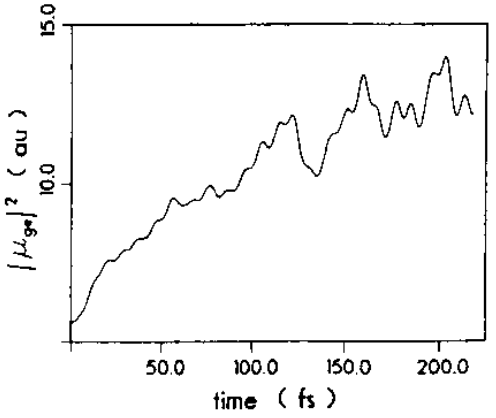

Fig. 10. Time evolution of the squared transition dipole, $|\mu_{ge}|^2$, between the ground and first excited state following transition to the excited state in $(H_2O)_{128}^-$. The transition dipole corresponding to the excited state configuration is larger because of the larger overlap between the corresponding wave functions.

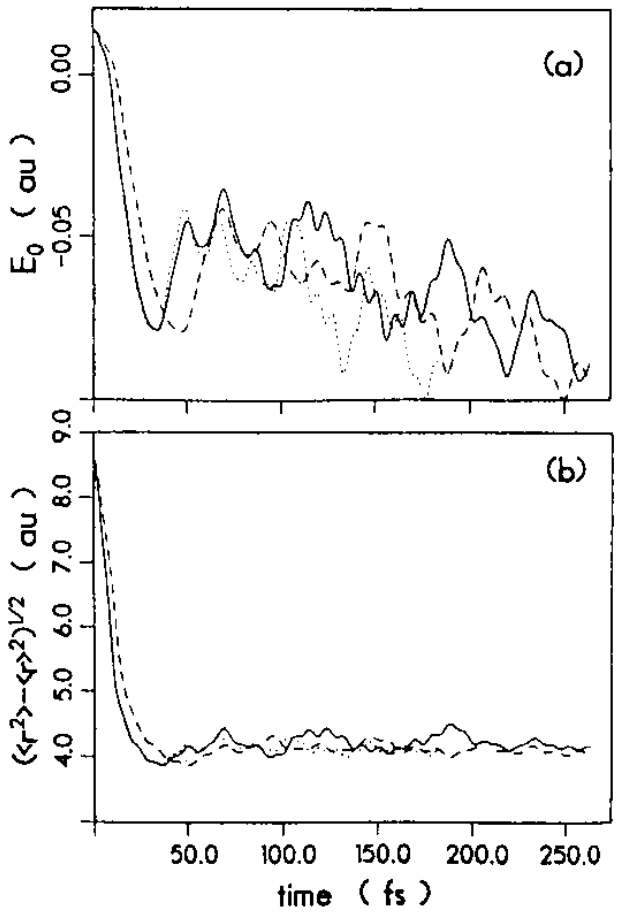

Fig. 11. a. Time evolution of the ground-state energy of an excess electron during an adiabatic localization process in *bulk* liquid water. At $t = 0$ the electron starts from a preexisting trap in a neutral water configuration. b. Time evolution of the width of the electronic wave functions, $((r^2) - (r)^2)^{1/2}$, during the same localization process. Solid lines = H_2O (256 molecules with periodic boundary conditions); dashed lines = D_2O. Both the H_2O and the D_2O trajectories start from the same initial configuration. The dotted lines in Figs. 11a and b correspond to the D_2O curve with the time axis divided by $\sqrt{2}$ (i.e., the deuterium to hydrogen mass ratio).

$|\mu_{ge}|^2$ between the ground and excited electronic states is shown in Fig. 10.

All these quantities exhibit a typical time evolution characterized by a very fast initial relaxation on a time scale of ~20–30 fs, followed by a slower relaxation process on a time scale of ~200–250 fs. A similar behavior is observed after a sudden switching back to the ground electronic state.

The slow (200–250-fs) component of the relaxation process seems to correspond to the longitudinal relaxation time (τ_L) of water, which is estimated to be in this range. The fast relaxation component is not predicted by continuum dielectric theories[94–104] or by approximate methods (such as the MSA)[63,106–110] which have been used to account for the microscopic solvent structure. In this context, we note that the behavior of the relaxation process observed in our simulations bears close resemblance to the simulation results of Rossky and Schnitker.[38] This similarity is emphasized in Fig. 11, where results of a simulation similar to that of Ref. 38, but using our models for the water–water interaction (RWK2-M) and for the electron–water pseudopotential, are shown. Figure 11a (solid curve) shows the time evolution of the ground-state energy of an electron starting in a preexisting trap in neutral bulk water (256 water molecules with periodic boundary conditions). In Fig. 11b (solid curve), we show the time evolution of the width of the electronic wave function for this process. As evident from Fig. 11b, $((r^2) - (r)^2)^{1/2}$ reaches essentially its equilibrium value of ~4 au after ~30 fs. We

note that a similar fast process was observed by us in a simulation of electron localization at the surface of a large (256) molecule water cluster.[32] It is interesting to note also that a similar behavior is observed in classical computer simulations of water relaxation about suddenly formed charge.[78,79,112]

To elucidate the nature of this fast relaxation process, we also show in Fig. 11 the relaxation behavior of D_2O during the electron localization process (dashed curves). The two curves corresponding to H_2O and D_2O in Fig. 11 start both from the same initial configuration. While statistics is obviously poor, it appears that the fast relaxation time in D_2O is longer by $\sqrt{2}$. This conclusion is emphasized by the dotted lines in Fig. 11a,b, where the results for D_2O are plotted vs. time scaled by $2^{-1/2}$, i.e., the hydrogen to deuterium mass ratio. Very similar behavior was obtained in comparing the fast relaxation process following electronic excitation in $(H_2O)_{128}^-$. We remark that it is experimentally known[115] that the Debye (as well as the longitudinal) relaxation time in D_2O is longer by $\sim 20\%$ than the corresponding times in H_2O.

Further insight into the fast relaxation process is gained by analyzing the relaxation dynamics in molecular shells about the excess electron. Such analysis shows that the fast relaxation process following electronic excitation of a solvated electron is primarily dominated by molecules nearest (i.e., within 7 au) to the center of the excess electron distribution. Furthermore, we find that the configurational changes that take place during this time are associated with rotations or vibrations of the water molecules nearest to the electron. Thus, after excitation the electronic charge distribution is more diffuse, resulting in a weakening of the electron–water interaction leading to a reorientational response of the molecules in the immediate vicinity of the excess electron, which is accomplished via rotations of the molecules (involving motion of the hydrogen atoms in an attempt to increase the degree of hydrogen bonding and the magnitude of the intermolecular interaction associated with them). That hydrogen bonding is disrupted in the first shell of water molecules by the presence of the electron is seen by the fact that the intermolecular interaction (per molecule) associated with the molecules in the second (7–10 au) shell is considerably larger than that associated with the first-shell molecules. We note that Maroncelli and Fleming[79] have reached similar conclusions from the analysis of their classical simulation data.

The isotope effect seen in Fig. 11 (and for the clusters) is indicative of the nature of this rotational response mechanism. We recall[116] that the Debye dielectric relaxation time, τ_D, obtained from a model of rotational diffusion is in our case independent of the rotator mass or its moment of inertia ($\tau_D = 4\pi\eta a^3/kT$, where η is the solvent viscosity and an appropriate choice for the "rotator radius" a is the O–H bond length). On the other hand, the rotational correlation function of free rotators in thermal equilibrium decays in time as $\sim e^{-t^2(kT/I)}$ where I is the moment of inertia.[116] We suggest that the dependence on $\sqrt{m_D/m_H} = \sqrt{2}$ seen from the isotope effect corresponds to the inertial character of this short-time relaxation. It would be interesting to check whether the temperature dependence of the fast relaxation time scales like $T^{-1/2}$ as also suggested by the free rotator model. However, in the present study we did not accumulate enough statistics to make a reliable check of this point.

Several other points concerning the observed relaxation behavior should be noted:

(a) The dynamics of electron localization and Stokes shift (reorganization energy) evolution are not sensitive to the cluster size for the (relatively large) water clusters that support an internally solvated electron ($n \gtrsim 60$), at least to within the statistical accuracy of our result for the relaxation time scales which we estimate to be ca. $\pm 20\%$. In contrast, the ground- and excited-state energies shift to more negative values for larger clusters and therefore we expect the IR absorption discussed below (see (g) and (h)) to peak at higher frequencies for larger clusters.

(b) Figure 7 and the results for deexcitation show that the excited-state electronic energy is much less sensitive to the reorganization of the surrounding water configuration than the ground-state energy. This is in contrast to the pronounced change in the widths (Fig. 9) of both the ground and excited electronic states following the electronic excitation. Underlying the water relaxation after transition to the excited electronic state is the weaker interaction with the more diffuse excited electronic charge distribution. Thus, the water molecules change their orientation in order to lower the intermolecular interaction energy. This water relaxation affects the electronic energy in two opposing ways: firstly, the electron–water interaction energy (the electron potential energy) is weakened (i.e., becomes less negative); secondly, the electron kinetic energy associated with the more diffuse wave function is smaller (less positive). The overall result is that there is only a very small net effect on the total excited state electronic energy.

(c) The similarity between the relaxation phenomena observed in the present work, in the electron localization simulation of Rossky and Schnitker,[38] and

in the classical simulations of Refs. 78, 79, and 112 is significant and surprising in view of the fact that not only different processes were studied, but mainly because very different models of water were used. We use the RWK2-M water–water potential[39] and the pseudopotential developed by Barnett et al.[25] for the water–electron interaction. In Ref. 38 the SPC water model was used, while in Refs. 78 and 79 the ST2 water model was employed. It appears that the inertial regime seen in all these simulations is not very sensitive to the details of the model used. This suggests that it is very probable that this behavior will be found in real water and perhaps in other associated solvents (with scaled characteristic times). It should be kept in mind, however, that all these studies are characterized by a non-self-consistent treatment of the electronic polarization of the solvent water molecules and that including such many-body contributions[117] may have some effect on the short-time behavior.[63]

(d) Another important difference between the (quantum-mechanical) processes simulated in the present work (and in Ref. 38) and the classical simulations of Refs. 78 and 79 is the fact that in the latter group of studies the charge distribution is held fixed after its instantaneous formation at $t = 0$, while in the electronic localization and relaxation studies the electronic charge distribution varies during the relaxation, mostly during the initial fast period. The fact that the time scales obtained from the quantum-mechanical simulations are similar to those seen in the classical, fixed-charge, studies again indicates that the dynamics is mainly driven by the inertial motion of the water molecules and that this motion is in a sense rate-determining also in the electronic relaxation and localization process. It should be emphasized that the fact that the electron charge distribution relaxes to practically its final form during the initial fast part of the relaxation process justifies the use of fixed-charge dielectric relaxation models for the longer time scales associated with electron localization, solvation, and transfer processes.

(e) Rao and Berne[78] and also Maroncelli and Fleming[79] have observed a very large jump of the average kinetic energy (temperature) of the classical atoms in the first solvation shell following the sudden charge formation. This local heating persists for a relatively long time (~ 0.5 ps). In our simulation, where the sudden electronic excitation or relaxation involves a relatively mild change in the charge distribution, no increase in the local temperature (beyond the noise level) was observed.

(f) Participation of intramolecular vibrational modes during the short-time stage of the relaxation processes discussed above cannot be ruled out. However, the similarity between the results obtained using our flexible water model and the other simulations which use rigid water molecules indicate that this relaxation channel does not play a major role in the process.

(g) It is interesting to speculate on the relation between the results obtained here and in Ref. 38 and the experimental results of Migus et al.[53] The fact that these authors do not observe a continuous blue shift of the absorption spectrum from the near IR to the 7000-Å range during the electron solvation process was interpreted by them (see also Ref. 38) as an indication of the existence of two species, one that absorbs in the near IR and the other which is the fully solvated electron. It is reasonable to assign the IR-absorbing species to the solvated electron in an excited state. Figure 12 gives a schematic view of the transitions involved. Our simulation results (see next section) give the peak of the excitation profile of the fully solvated electron at ~ 2.1 eV and the vertical transition between the first excited state and the delocalized continuum at slightly above 1 eV. The experimental result for the former is ~ 1.7 eV. The fact that our simulations tend to overestimate the transition energies leads us to suggest that the vertical transition from the excited states to the delocalized continuum may peak below 1 eV. In the present work, we have determined the relaxation proc-

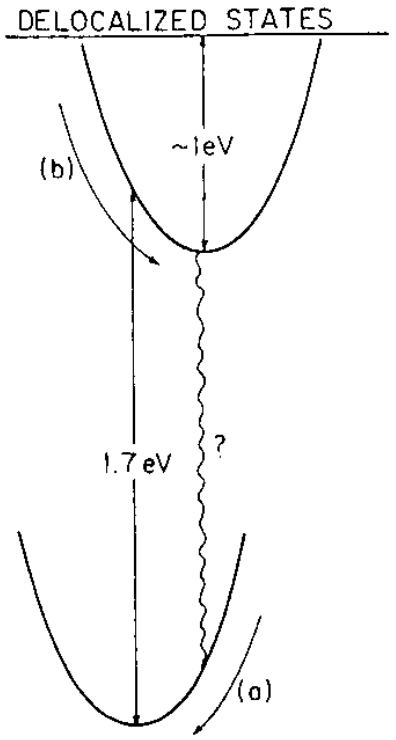

Fig. 12. A schematic description of a model for the time scales and energetics associated with the dynamics of electron solvation and excitation in water.

esses (a) and (b) of Fig. 12 to occur on similar time scales and to involve at least two relaxation times, ca. 30 fs and 200 fs. It is likely that the 110-fs process that Migus et al.[53] attribute to the growth of the IR-absorbing species actually reflects the evolution of a blue shift of the IR absorption by the excited state of the solvated electron, to the delocalized continuum, *during* the relaxation process (b). The time (240 fs) observed by these workers for the decay of the IR-absorbing species and the buildup of the fully solvated electron are probably due to the relaxation process (a) in Fig. 12, to a radiationless transition from the excited to the ground state (denoted by a question mark in Fig. 12), or to a combination of both. It will be highly desirable to determine from the theoretical model the rate of this nonadiabatic radiationless process.

(h) The model described above and the simulation results of this paper lead us to predict that following excitation of the solvated electron in water one should be able to observe a transient IR absorption that will peak below 1 eV and will decay on the 240-fs time scale observed by Migus et al.[53] This absorption should in principle blue-shift on a time scale characterized by a 20–30-fs process and a slower $\sim$ 200-fs process (process (b) of Fig. 12). The short-time blue shift will be sensitive to deuterium isotope substitution of the water in the way described above. We should note, however, that the very weak dependence of the excited state energy E_1 on the solvent reorganization following the transition from the ground to the excited state (see point (b) above) suggests that this blue shift may be too weak to be observed.

(i) A substantial part of the water relaxation in response to the charge reorganization (electron excitation or localization as well as classical charge formation) observed here and in other works is beyond the prediction of current theoretical treatments of solvation dynamics. It is highly significant that the classical simulation by Maroncelli and Fleming[111] indicates that the essential features of this phenomenon can be described within linear response theory. This suggests that a linear response based calculation of the wavevector and frequency-dependent dielectric response $\varepsilon(k, \omega)$ for associated liquids should be a sufficient theoretical framework for describing this phenomenon. A recent calculation[106] of $\varepsilon(k, \omega)$ for a model of polarizable atoms on a lattice (as an approximation for a nonassociated solvent) yields only the (nonexponential) slow time scale relaxation with characteristic times between τ_D and $\varepsilon_L = (\varepsilon_\infty/\varepsilon_0)/\tau_D$. This indicates the importance of structural reorganization within the first solvation shell characteristic of associated solvents in the initial fast stage of the relaxation.

5. SPECTRA OF EXCESS ELECTRONS IN CLUSTERS

Determination of the excess electron spectral lineshapes requires monitoring of the excited states throughout the dynamical propagation of the coupled quantum-classical system which evolves on the ground electronic potential energy surface. This can be achieved using the GSD method by application of the projection operator technique described in Section 2.

Contour plots of the ground- and excited-state excess electron distributions, obtained for a randomly chosen configuration drawn from the equilibrium ensemble at 300 K of an internally localized state of an excess electron in a $(H_2O)_{64}^-$ cluster, are shown in Fig. 13. The ground-state distribution shown in Fig. 13a,b has s-like character, while the distributions for the three lowest excited states (Fig. 13c,e,f) are p-like (the three-dimensional plot corresponding to Fig. 13c is shown in Fig. 13d). Note, however, that the marked deviations from spherical symmetry of the molecular environment of the excess electron are reflected in the splitting of the excited-state energy levels and in the shapes of the corresponding electron distributions (see also Ref. 114).

Underlying the spectral lineshape of the localized excess electron are the fluctuations in the values of the ground and excited states due to the finite-temperature dynamical variations in the molecular environment coupled to the solvated electron. Consequently, the extraction of spectral information from the simulations requires extensive averaging over the dynamically generated equilibrium phase-space trajectories of the system. As an example, we show in Fig. 14 the absorption lineshape for an internally localized state of an excess electron in a $(H_2O)_{256}^-$ cluster, at 300 K. This result is based on 0.5-ps trajectories for three simulations which started from different initial conditions. The spectra shown in Fig. 14 were obtained by weighting the excitation energies by the transition dipoles, $|\mu_{gi}|^2$ ($i = 1, 2, 3$ and g denoting the ground state) along the GSD trajectories of the system.

The electronic absorption spectrum, which is primarily associated with overlapping transitions from the (s-like) ground state to the three (p-like) lowest excited states, is only slightly sensitive (observed differences are within our noise bounds of $\sim$ 10%) to the cluster size in the range $n = 64$–256 water molecules. The calculated absorption peak is at $\sim$ 2.1 eV and has a width of $\sim$ 1 eV (experimental results[43] for bulk water are 1.72 eV and 0.92 eV, respectively), and the results are close to those obtained by Schnitker et al.[114] for a bulk system (several hundred molecules with periodic boundary conditions). The similarity between these results is striking in view of the fact that different (though physically reason-

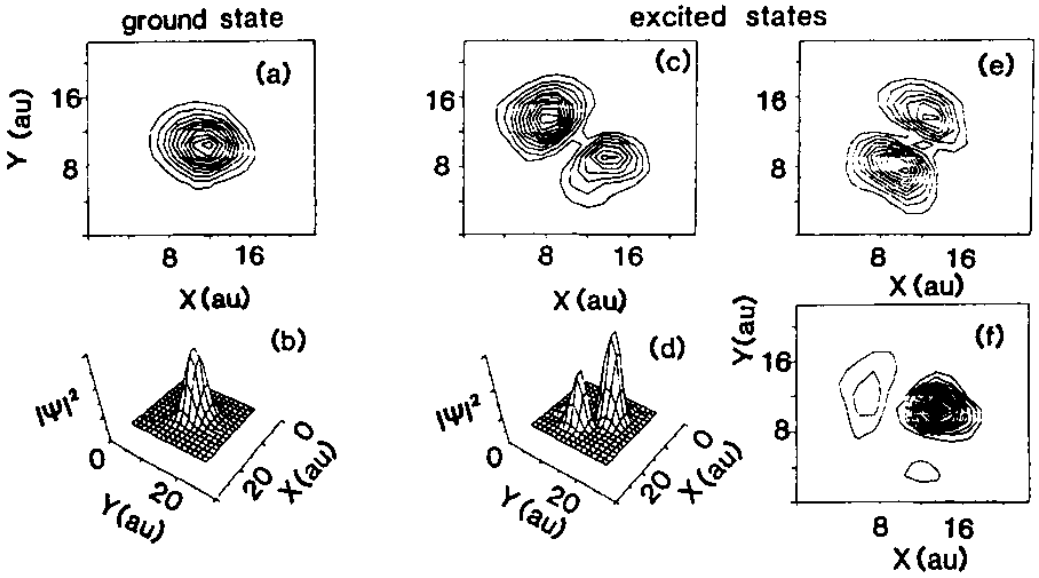

Fig. 13. Two- and three-dimensional contours of the excess electron density in the ground state (a, b) and three lowest excited states (c–f) in the $(H_2O)_{64}^-$ cluster. The three-dimensional contour in Fig. 13d corresponds to the two-dimensional one shown in Fig. 13c. Note the p-character of the excited states. All contours are calculated in the *xy* plane at the middle of the *z* axis of the calculational cell. Distances are in atomic units.

able) potentials were used for the water–water and the water–electron interactions, suggesting that the gross features of the electron transition spectra are not very sensitive to the details of these potentials. Romero and Jonah[118] have recently reached a similar conclusion, after obtaining a similar spectrum using a simpler model.

The fact that similar electronic spectra are obtained using the SPC water potential[114,119] which describes rigid water molecules, and, in our work, the RWK2-M potential[39] which accounts also for intramolecular motion, demonstrates that the electronic absorption spectra are not sensitive to the intramolecular water motions.

To further illustrate the use of quantum simulation methods in investigations of the dynamics and spectra of molecular and condensed-phase systems, we present most recent results concerning an excess electron in small alkali-halide clusters.[120] In previous studies, employing the QUPID simulations,[19–22] we have investigated the compositional, structural, and size dependence of various electron localization modes in ionic alkali-halide clusters. In these studies, the interionic interactions are given by the Born–Mayer potentials, and the electron interaction consists of a sum of electron–ion pseudopotentials. Thus $\phi_{eX^-} = e^2/r$ for the electron–anion interaction, while the electron–cation interactions are given by $\phi_{eM^+}(r) = -e^2/R_c$ for $r \leqq R_c$ and $\phi_{eM^+}(r) = -e^2/r$ for $r > R_c$. (For Na^+, $R_c = 3.22a_0$).

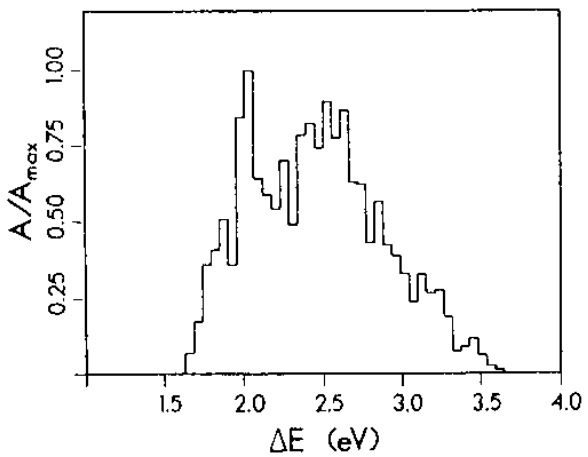

Fig. 14. Absorption spectral lineshape for an excess electron in $(H_2O)_{256}^-$, obtained via GSD simulations at 300 K. Energy in eV.

The QUPID simulations[19–22] revealed a systematic dependence of the mode of electron localization (surface vs. internal) on the size of the clusters, thus establishing patterns pertaining to the structure, energetics, and abundances related to electron attachment and localization to finite F-center systems. Furthermore, cluster-induced isomerization phenomena have been investigated.[21]

In the current study, we focus on the spectroscopy of small alkali-halide molecules $[(NaX_2)^+ + e^-]$, where X = Cl or F, explored via the GSD method discussed in Section 2. The absorption spectral lineshapes of Na_2Cl and Na_2F obtained via GSD simulations at 100 K are shown in Figs. 15 and 16. In these studies, the Born–Mayer (BM) potentials with the parametrization due to Fumi and Tosi (FT)[121] were used for Na_2Cl and the Born and Huang (BH) potentials[122] were used for Na_2F. The adiabatic ionization energies for the clusters are

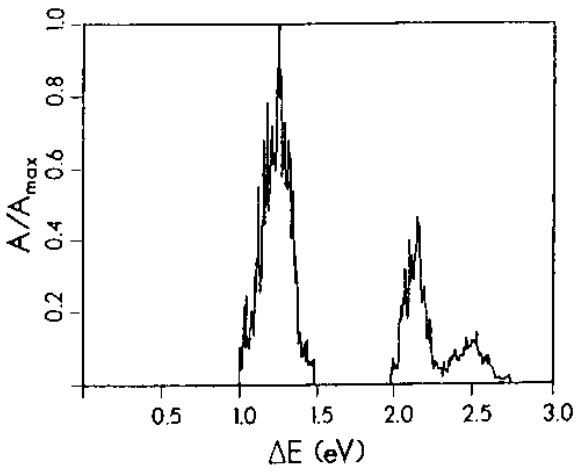

Fig. 15. Absorption spectral lineshape for an excess electron in Na_2Cl obtained via GSD simulations at 100 K. Energy in eV.

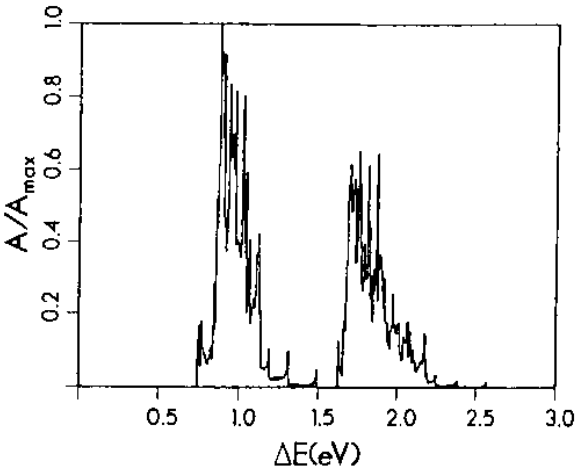

Fig. 16. Absorption spectral lineshape for an excess electron in Na_2F obtained via GSD simulations at 100 K. Energy in eV.

-3.63 eV and -3.47 eV for chloride and fluoride clusters, respectively, in adequate agreement with recent measurements[10c,d,123,124] and Hartree–Fock calculations[125] for Na_2Cl. The equilibrium structures of the ground-state clusters are shown in Figs. 17 and 18, where the equilibrium-averaged configurations are given. We note that the linear $[Na_2X]^+$ (X = Cl or F) clusters change to quadrilateral structures upon excess electron attachment. Furthermore, the equilibrium Na–X–Na angle in the chloride cluster is 85.7°, while the fluoride is more open with an angle of 110°.

In addition to the electronic spectra,[120,126] the localization of an excess electron in a cluster allows interrogation of the vibrational dynamics of the cluster. In Fig. 19 the vibrational densities of states of Na_2Cl, obtained via Fourier transformation of the velocity autocorrelation function, are shown along with the density of states (solid line) for the ionized cluster, $[Na_2Cl]^+$. The next to lowest frequency corresponds to the bending mode of the cluster and the two highest frequencies to NaCl stretch and antistretch vibrations (the peak in $D(\omega)$, centered at $\omega = 0$, corresponds to rotations of the cluster). It is interesting to note that the two stretch modes shift to lower frequency upon electron attachment, while the bending mode shifts to a higher frequency. The pattern of frequency shifts correlates with partial screening of the alkali cations by the excess electron, which brings about a decrease in the stretch vibrational frequency, while the localization of the excess electron opposite the halogen anion (see Fig. 17) hinders the

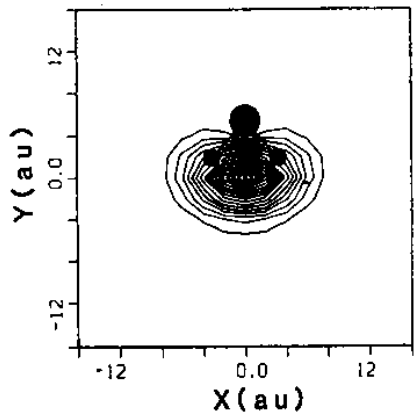

Fig. 17. Contour plot of the ground-state excess electron distribution and equilibrium atomic configuration of Na_2Cl at 100 K. In the equilibrium average configuration, the Na–Cl bond length is 4.73 ± 0.09 au and the distance between the Cl^- anion and the center of the excess electron charge density is 5.39 ± 0.08 au. The Na–Cl–Na angle is $85.7° \pm 2.9°$. The maximum contour corresponds to $4.36 \times 10^{-3}\ e/a_0^3$, and the increment between contours is $2.72 \times 10^{-4}\ e/a_0^3$. Contours are in the plane of the cluster through the atoms and distances are in Bohr radii.

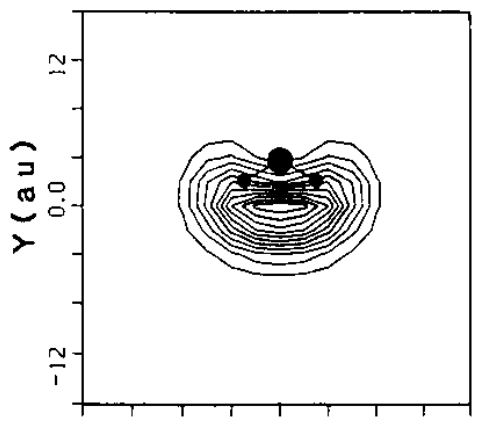

Fig. 18. Same as Fig. 17 for Na_2F at 100 K. In the equilibrium averaged configuration, the Na–F bond length is 3.71 ± 0.11 au, and the distance between the anion and the center of the excess electron charge density is 4.28 ± 0.15 au. The Na–F–Na angle is $110.5° \pm 4.9°$. The maximum contour corresponds to $3.09 \times 10^{-3}\ e/a_0^3$, and the increment between contours is $2.57 \times 10^{-4}\ e/a_0^3$. Contours are in the plane of the cluster through the atoms and distances are in Bohr radii.

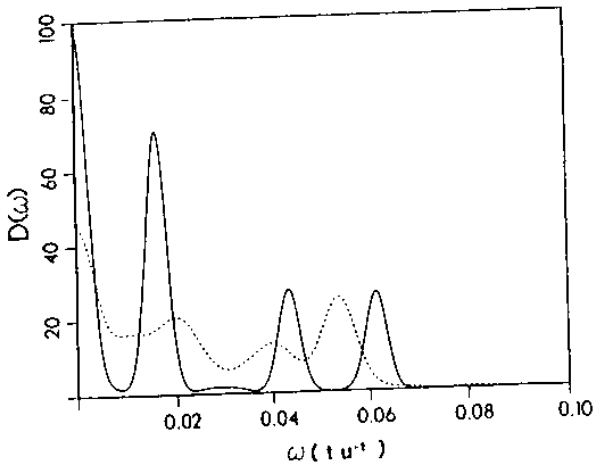

Fig. 19. Total vibrational density of state, $D(\omega)$, vs. ω, obtained via a GSD simulation of Na_2Cl at 100 K (dashed line). $D(\omega)$ for $[Na_2Cl]^+$ obtained via a classical simulation at 100 K is denoted by a solid line. ω in 9.7×10^{14} s^{-1}. Note the shift of the bending mode in Na_2Cl to a higher frequency and the decrease in frequency of the stretch modes.

motion of the anion resulting in an increase of the bending-mode frequency.

Acknowledgment. This work is supported by the U.S. Department of Energy under Grant No. DE-FG05-86ER-45234, (to U.L.), the U.S.–Israel Binational Science Foundation and the Commission for Basic Research of the Israel Academy of Science (to A.N.). Fruitful collaboration on the path-integral simulations and numerous discussions throughout with Joshua Jortner are gratefully acknowledged.

REFERENCES

(1) (a) Armbuster, M.; Haberland, H.; Schindler, H.G. *Phys. Rev. Lett.*, 1981, **47**: 323. (b) Haberland, H.; Langosch, H.; Schindler, H.G.; Worsnop, D.R. *Surf. Sci.*, 1985, **156**: 517.

(2) (a) Posey, L.A.; Johnson, M.A. *J. Chem. Phys.*, 1988, **89**: 4807. (b) Posey, L.A.; DeLuca, M.J.; Campagnola, P.J.; Johnson, M.A. *J. Phys. Chem.*, 1989, **93**: 1178.

(3) Haberland, H.; Schindler, H.G.; Worsnop, D.R. *Ber. Bunsenges. Phys. Chem.*, 1984, **88**: 270.

(4) Haberland, H.; Schindler, H.G.; Worsnop, D.R. *J. Chem. Phys.*, 1984, **81**: 3742.

(5) Knapp, M.; Echt, O.; Kreisle, D.; Recknagel, E. *J. Chem. Phys.*, 1986, **85**: 636; *J. Phys. Chem.*, 1987, **91**: 2601.

(6) (a) Bowen, K.H.; Eaton, J.G. In *The Structure of Small Molecules and Ions*; Naaman, R.; Vager, Z., Eds.; Plenum Press: New York, 1988; p. 147. (b) Arnold, S.T.; Eaton, J.G.; Patel-Misra, D.; Sarkas, H.W.; Bowen, K.H. In *Ion Cluster Spectroscopy and Structure*; Maier, J.P., Ed.; Elsevier: Amsterdam, 1989.

(7) See articles in *Elemental and Molecular Clusters*; Benedek, G.; Martin, T.P.; Pacchioni, G., Eds.; Springer-Verlag: Berlin, 1988.

(8) Miller, T.M.; Leopold, D.G.; Murray, K.K.; Lineberger, W.C. *J. Chem. Phys.*, 1986, **85**: 2368, and references therein.

(9) Martin, T.P. *Phys. Rep.*, 1983, **95**: 167, and references therein.

(10) (a) Kappes, M.; Radi, P.; Schar, M.; Schumacher, E. *Chem. Phys. Lett.*, 1985, **113**: 243. (b) Peterson, K.I.; Dao, P.D.; Castelman, A.W., Jr. *J. Chem. Phys.*, 1983, **79**: 777. (c) Honea, E.C.; Homer, M.L.; Labastie, P.; Whetten, R.L. *Phys. Rev. Lett.*; 1989, **63**: 394. (d) Kappas, M.; to be published.

(11) (a) Newton, M. *J. Chem. Phys.*, 1973, **58**: 5833. (b) Rao, B.K.; Kestner, N.R. *J. Chem. Phys.*, 1984, **80**: 1587.

(12) Chipman, D.J. *J. Phys. Chem.*, 1978, **82**: 1980; 1979, **83**: 1657.

(13) (a) Bennemann, K.H.; Stampfli, P. *Phys. Rev. Lett.*, 1987, **58**: 2635. (b) Stampfli, P.; Bennemann, K.H. *Phys. Rev. A*, 1988, **71**: 1674.

(14) Jordan, K.D. *Acc. Chem. Res.*, 1979, **12**: 36.

(15) See Refs. 1–14 in Ref. 8.

(16) (a) Nabutovskii, V.M.; Romanov, D.A. *Sov. J. Low Temp. Phys.*, 1985, **11**: 277. (b) Rama Krishna, M.V.; Whaley, K.B. *Phys. Rev. B*, 1988, **38**: 11839.

(17) Wallqvist, A.; Thirumalai, D.; Berne, B.J. *J. Chem. Phys.*, 1986, **85**: 1583.

(18) See reviews by (a) Berne, B.J.; Thirumalai, D. *Annu. Rev. Phys. Chem.*, 1986, **37**: 401; (b) Sprik, M.; Klein, M. *Comput. Phys. Rep.*, 1988, **7**: 147.

(19) See reviews by (a) Landman, U.; Barnett, R.N.; Cleveland, C.L.; Luo, J.; Scharf, D.; Jortner, J. In *Few Body Systems and Multiparticle Dynamics*; Micha, D., Ed.; AIP: New York, 1987; p. 200. (b) Landman, U. In *Recent Developments in Computer Simulation Studies in Condensed Matter Physics*; Landau, D.P.; Mon, K.K.; Schuttler, H.B., Eds.; Springer-Verlag: Berlin, 1988; p. 144.

(20) See reviews by (a) Jortner, J.; Scharf, D.; Landman, U. in Ref. 7, p. 148; (b) Barnett, R.N.; Landman, U.; Scharf, D.; Jortner, J. *Acc. Chem. Res.*, 1989, **22**: 350.

(21) Scharf, D.; Jortner, J.; Landman, U. *J. Chem. Phys.*, 1988, **88**: 4273.

(22) Landman, U.; Scharf, D.; Jortner, J. *Phys. Rev. Lett.*, 1985, **54**: 1860.

(23) Barnett, R.N.; Landman, U.; Cleveland, C.L.; Jortner, J. *Phys. Rev. Lett.*, 1987, **59**: 811.

(24) (a) Landman, U.; Barnett, R.N.; Cleveland, C.L.; Scharf, D.; Jortner, J. *J. Phys. Chem.*, 1987, **91**: 4890. (b) Barnett, R.N.; Landman, U.; Dhar, S.; Kestner, N.R.; Jortner, J.; Nitzan, A. *J. Chem. Phys.*, 1989, **91**: 7797.

(25) Barnett, R.N.; Landman, U.; Cleveland, C.L.; Jortner, J. *J. Chem. Phys.*, 1988, **88**: 4421.

(26) Barnett, R.N.; Landman, U.; Cleveland, C.L.; Jortner, J. *J. Chem. Phys.*, 1988, **88**: 4429.

(27) Barnett, R.N.; Landman, U.; Jortner, J. *Chem. Phys. Lett.*, 1988, **145**: 382.

(28) Barnett, R.N.; Landman, U.; Kestner, N.R.; Jortner, J. *J. Chem. Phys.*, 1988, **88**: 6670; *Chem. Phys. Lett.*, 1988, **148**: 249.

(29) Barnett, R.N.; Landman, U.; Nitzan, A. *Phys. Rev. A*, 1988, **38**: 2178.
(30) (a) Barnett, R.N.; Landman, U.; Nitzan, A. *J. Chem. Phys.*, 1988, **89**: 2242. (b) Barnett, R.N.; Landman, U.; Nitzan, A.; to be published.
(31) Jortner, J.; Landman, U.; Barnett, R.N. *Chem. Phys. Lett.*, 1988, **152**: 353.
(32) Barnett, R.N.; Landman, U.; Nitzan, A. *Phys. Rev. Lett.*, 1989, **62**: 106; see also *J. Chem. Phys.*, 1989, **91**: 5567.
(33) Barnett, R.N.; Landman, U.; Nitzan, A. *J. Chem. Phys.*, 1989, **90**: 4413.
(34) Marchi, M.; Sprik, M.; Klein, M.L. *J. Chem. Phys.*, 1988, **89**: 4918.
(35) Martyna, G.J.; Berne, B.J. *J. Chem. Phys.*, 1988, **88**: 4516; 1989, **90**: 3744.
(36) (a) Feit, M.D.; Feit, J.A., Jr.; Steiger, A. *J. Comput. Phys.*, 1982, **47**: 412. (b) Feit, M.D.; Fleck, J.A., Jr. *J. Chem. Phys.*, 1983, **78**: 301; 1984, **80**: 2578. (c) Kosloff, D.; Kosloff, R. *J. Comput. Phys.*, 1983, **53**: 35. (d) See review by Kosloff, R. *J. Phys. Chem.*, 1988, **92**: 2087.
(37) (a) Dirac, P.A.M. *Proc. Cambridge Philos. Soc.*, 1930, **26**: 376. (b) Kumamoto, D.; Sibey, R. *J. Chem. Phys.*, 1981, **75**: 5164.
(38) See review by Rossky, P.J.; Schnitker, J. *J. Phys. Chem.*, 1988, **92**: 4277.
(39) For water, we use the RWK2-M potential. See Reimers, J.R.; Watts, R.O. *Chem. Phys.*, 1984, **85**: 83; 1982, **64**: 95; see also Ref. 25.
(40) For the intermolecular interaction in ammonia, we use the potential (Model C) developed by Hinchliffe, A.; Bounds, D.G.; Klein, M.L.; McDonald, I.R.; Righini, R. *J. Chem. Phys.*, 1981, **74**: 1211, supplemented by intramolecular interactions modeled via a harmonic valence-coordinate model potential based on the one discussed by Herzberg, G. in *Infrared and Raman Spectra*; Van Nostrand-Reinhold: New York, 1945; table 43, p. 177.
(41) The interatomic interactions which we employed in simulations of ionic clusters are discussed in Scharf, D.; Landman, U.; Jortner, J. *Chem. Phys. Lett.*, 1986, **130**: 5504; see also Refs. 19–22.
(42) Schnitker, J.; Rossky, R.J. *J. Chem. Phys.*, 1987, **86**: 3462, 3471.
(43) Hart, E.J.; Gottschell, W.C. *J. Am. Chem. Soc.*, 1969, **71**: 2101.
(44) (a) Selloni, A.; Carenvali, P.; Car, R.; Parrinello, M. *Phys. Rev. Lett.*, 1987, **59**: 823, and Refs. 5–8 therein. (b) See also Thirumalai, D.; Bruskin, E.J.; Berne, B.J. *J. Chem. Phys.*, 1985, **83**: 230.
(45) Kosloff, R.; Talezer, H. *Chem. Phys. Lett.*, 1986, **127**: 223.
(46) Douglass, C.H., Jr.; Weil, D.A.; Charlier, P.A.; Eades, R.A.; Truhlar, D.C.; Dixon, D.A. In *Chemical Applications of Atomic and Molecular Electrostatic Potentials*; Politzer, P.; Truhlar, D.G., Eds.; Plenum: New York, 1981; p. 173.
(47) Kerr, C.W.; Karplus, M. In *Water*; Frank, F., Ed.; Plenum: New York, 1972; p. 21.
(48) (a) Bardsley, J.N. *Case Stud. At. Phys.*, 1974, **4**: 299. (b) Kleiman, G.G.; Landman, U. *Phys. Rev. B*, 1973, **8**: 5484.
(49) Truhlar, D.G., in Ref. 46, p. 123.
(50) See review by McLendon, G. *Acc. Chem. Res.*, 1988, **21**: 160, and references therein.
(51) See review by (a) Simon, J.D. *Acc. Chem. Res.*, 1988, **21**: 128; (b) Maroncelli, M.; Castner, E.W., Jr.; Webb, S.P.; Fleming, G.R. In *Ultra-Fast Phenomena*, Vol. 5; Fleming, G.R.; Siegman, A.E., Eds.; Springer-Verlag: Berlin, 1986; p. 303, and references therein.
(52) *Electrons in Fluids, Colloque Wely III*; Jortner, J.; Kestner, N.R., Eds.; Springer-Verlag: Heidelberg, 1973.
(53) Migus, A.; Gauduel, Y.; Martin, J.L.; Antonetti, A. *Phys. Rev. Lett.*, 1987, **58**: 1559, and references therein.
(54) Kenney-Wallace, G.A.; Jonah, C.D. *J. Phys. Chem.*, 1982, **86**: 2572.
(55) Wiesenfeld, J.M.; Ippen, E.P. *Chem. Phys. Lett.*, 1980, **73**: 47.
(56) (a) Kenney-Wallace, G.A. *Adv. Chem. Phys.*, 1981, **47**: 535. (b) Kenney-Wallace, G.A. In *Picosecond Phenomena*; Shank, C.V.; Ippen, E.P.; Shapiro, S.L., Eds.; Springer-Verlag: Berlin, 1978.
(57) Schnitker, J.; Rossky, P.J.; Kenney-Wallace, G.A. *J. Chem. Phys.*, 1986, **85**: 2986.
(58) Motakabbir, K.A.; Rossky, P.J. *Chem. Phys.*, 1988, **129**: 253.
(59) Robinson, G.W.; Thistlethwaite, P.J.; Lee, J. *J. Phys. Chem.*, 1986, **90**: 4224.
(60) (a) Krohn, C.E.; Antoniewic, P.R.; Thompson, J.C. *Surf. Sci.*, 1980, **101**: 241. (b) Bennett, G.T.; Thompson, J.C. *J. Chem. Phys.*, 1986, **84**: 1901.
(61) Rentzepis, P.M.; Jones, R.P.; Jortner, J. *J. Chem. Phys.*, 1973, **59**: 766; *Chem. Phys. Lett.*, 1972, **15**: 480.
(62) Walker, D.C. *J. Phys. Chem.*, 1980, **84**: 1140.
(63) Callef, D.F.; Wolynes, P.G. *J. Chem. Phys.*, 1983, **78**: 4145.
(64) Hubbard, J.B.; Wolynes, P.G. In *Physics of Ionic Solvation*; Ulstrup, J., Ed.; Elsevier: Amsterdam, 1986.
(65) See, for example, the papers in *Faraday Discuss. Chem. Soc.*, 1988, **85** for a survey of current areas of research.
(66) Kosower, E.M., Huppert, B. *Annu. Rev. Phys. Chem.*, 1986, **37**: 127.
(67) Ware, W.R.; Lee, S.K.; Chow, P. *Chem. Phys. Lett.*, 1968, **2**: 356.
(68) Ware, W.R.; Lee, S.K.; Brandt, C.J.; Chow, P.P. *J. Chem. Phys.*, 1971, **54**: 4729.
(69) Hallidy, L.A.; Topp, M.R. *Chem. Phys. Lett.*, 1977, **48**: 41.
(70) Mazurenko, Yu.T.; Udaltsov, V.S. *Opt. Spectrosc. (USSR)*, 1978, **44**: 417.
(71) Okamura, T.; Sumitani, M.; Yoshihara, K. *Chem. Phys. Lett.*, 1983, **94**: 339.
(72) Yeh, S.W.; Phillips, L.A.; Webb, S.P.; Buhse, L.F.; Clark, J.H. In *Ultrafast Phenomena*, Vol. 4; Auston, D.H.; Eisenthal, K.B., Eds.; Springer-Verlag: Berlin, 1984; p. 359.

(73) Maroncelli, M.; Fleming, G.R. *J. Chem. Phys.*, 1987, **86**: 6221.
(74) Nagarajan, V.; Brearley, A. M.; Kang, T.J.; Barbara, P.F. *J. Chem. Phys.*, 1987, **86**: 3183.
(75) Kahlow, M.A.; Kang, T.J.; Barbara, P.F. *J. Phys. Chem.*, 1987, **91**: 6452.
(76) Kahlow, M.A.; Kang, T.J.; Barbara, P.F. *J. Chem. Phys.*, 1988, **88**: 2372.
(77) Calef, D.F.; Wolynes, P.G. *J. Phys. Chem.*, 1983, **87**: 3387; *J. Chem. Phys.*, 1983, **78**: 470.
(78) Rao, M.; Berne, B.J. *J. Phys. Chem.*, 1981, **85**: 1498.
(79) Maroncelli, M.; Fleming, G.R. *J. Chem. Phys.*, 1988, **89**: 5044.
(80) Struve, W.S.; Rentzepis, P.M. *Chem. Phys. Lett.*, 1974, **29**: 23; *J. Chem. Phys.*, 1974, **60**: 1533.
(81) Huppert, D.; Rand, S.D.; Rentzepis, P.M.; Barbara, P.F.; Struve, W.S.; Grabowski, Z.R. *J. Chem. Phys.*, 1981, **75**: 5714.
(82) Wang, Y.; McAuliffe, M.; Novak, F.; Eisenthal, K.B. *J. Phys. Chem.*, 1981, **85**: 3736.
(83) Huppert, D.; Kanety, H.; Kosower, E.M. *Discuss. Faraday Soc.*, 1982, **74**: 161.
(84) Kosower, E.M.; Huppert, D. *Chem. Phys. Lett.*, 1983, **96**: 433.
(85) Huppert, D.; Ittah, V.; Kosower, E.M. *Chem. Phys. Lett.*, 1988, **144**: 15.
(86) Castner, E.W., Jr.; Maroncelli, M.; Fleming, G.R. *J. Chem. Phys.*, 1987, **86**: 1090.
(87) (a) Su, S.G.; Simon, J.D. *J. Phys. Chem.*, 1986, **90**: 6475. (b) *J. Phys. Chem.*, 1987, **91**: 2693. (c) Simon, J.D.; Su, S.G. *J. Chem. Phys.*, 1987, **87**: 7016.
(88) Heitele, H.; Michel-Beyerle, M.E.; Finckh, P. *Chem. Phys. Lett.*, 1987, **138**: 237.
(89) Baxendale, J.H.; Wardman, P. *Nature*, 1971, **230**: 449; *J. Chem. Soc. Faraday Trans. 1*, 1973, **69**: 584; *Can. J. Chem.*, 1977, **55**: 1996.
(90) Chase, W.J.; Hunt, J.W. *J. Phys. Chem.*, 1975, **79**: 2835.
(91) Kenney-Wallace, G.A.; Jonah, C.D. *Chem. Phys. Lett.*, 1976, **39**: 596.
(92) Miyasaka, H.; Masuhara, H.; Mataga, N. *Laser Chem.*, 1987, 7: 119.
(93) Kenney-Wallace, G.A.; Hall, G.E.; Hunt, L.A.; Sarantidis, K. *J. Phys. Chem.*, 1980, **84**: 1145.
(94) (a) Sumi, H.; Marcus, R.A. *J. Chem. Phys.*, 1986, **84**: 4894. (b) Nadler, W.; Marcus, R.A. *J. Chem. Phys.*, 1987, **86**: 3906.
(95) Bergsma, J.P.; Gertner, B.J.; Wilson, K.R.; Hynes, J.T. *J. Chem. Phys.*, 1987, **86**: 1356.
(96) Gertner, B.J.; Bergsma, J.P.; Wilson, K.R.; Lee, S.; Hynes, J.T. *J. Chem. Phys.*, 1987, **86**: 1377.
(97) Rips, I.; Jortner, J. *J. Chem. Phys.*, 1987, **87**: 2090.
(98) Zichi, D.A.; Hynes, J.T. *J. Chem. Phys.*, 1988, **88**: 2513.
(99) Sparpaglione, M.; Mukamel, S. *J. Chem. Phys.*, 1988, **88**: 3263.
(100) Mazurenko, Yu.T. *Opt. Spectrosc. (USSR)*, 1974, **36**: 283.
(101) Bagchi, B.; Oxtoby, D.W.; Fleming, G.R. *Chem. Phys.*, 1984, **86**: 257.
(102) van der Zwan, G.; Hynes, J.T. *J. Phys. Chem.*, 1985, **89**: 4181.
(103) Loring, R.F.; Yan, Y.J.; Mukamel, S. *Chem. Phys. Lett.*, 1987, **135**: 23.
(104) Castner, E.W., Jr.; Bagchi, B.; Fleming, G.R. *Chem. Phys. Lett.*, 1988, **143**: 270.
(105) Castner, E.W., Jr.; Fleming, G.R.; Bagchi, B.; Maroncelli, M. *J. Chem. Phys.*, 1988, **89**: 3519.
(106) (a) Loring, R.F.; Mukamel, S. *J. Chem. Phys.*, 1987, **87**: 1272. (b) Loring, R.F.; Yan, Y.T.; Mukamel, S. *J. Chem. Phys.*, 1987, **87**: 5840.
(107) Friedrich, V.; Kivelson, D. *J. Chem. Phys.*, 1987, **86**: 6425.
(108) Wolynes, P.G. *J. Chem. Phys.*, 1987, **86**: 5133.
(109) Rips, I.; Klafter, J.; Jortner, J. *J. Chem. Phys.*, 1988, **88**: 3246; *J. Chem. Phys.*, 1988, **89**: 4288.
(110) Nichols, A.L. III; Calef, D.F. *J. Chem. Phys.*, 1988, **89**: 3783.
(111) Maroncelli, M.; Fleming, G.R. *J. Chem. Phys.*, 1988, **89**: 875.
(112) (a) Engstrom, S.; Jonsson, B.; Impey, R.W. *J. Chem. Phys.*, 1984, **80**: 5481. (b) Engstrom, S.; Jonsson, B. *J. Magn. Reson.*, 1982, **50**: 1.
(113) Karim, O.A.; Haymet, A.D.J.; Banet, M.J.; Simon, J.D. *J. Phys. Chem.*; submitted for publication.
(114) Schnitker, J.; Motakabbir, K.; Rossky, P.J.; Friesner, R. *Phys. Rev. Lett.*, 1988, **60**: 456.
(115) Collie, C.H.; Hasted, J.B.; Ristoy, D.M. *Proc. Phys. Soc.*, 1948, **60**: 145.
(116) Bottcher, C.J.F.; Bordewijk, P. *The Theory of Electric Polarization*, Vol. 2, Chapter 11; Elsevier: Amsterdam, 1978.
(117) Wallqvist, A.; Thirumalai, D.; Berne, B.J. *J. Chem. Phys.*, 1987, **86**: 6404.
(118) Romero, C.; Jonah, C.D. *J. Chem. Phys.*, 1989, **90**: 1877.
(119) Berendsen, H.J.D.; Postma, J.P.M.; Von Gunstren, W.I.; Hermans, J. In *Intermolecular Forces*; Pullman, B., Ed.; Reidel: Dordrecht, 1981.
(120) Rajagopal, G.; Barnett, R.N.; Landman, U.; Nitzan, A.; to be published.
(121) Fumi, F.G.; Tosi, M.P.; *J. Phys. Chem. Solids*, 1964, **25**: 31, 45.
(122) Born, M.; Huang, K. *Dynamical Theory of Crystal Lattices*; Oxford University Press: London, 1954.
(123) For Na_2Cl the experimental value for the vertical ionization potential is 4.1 ± 0.1 eV; see references 10a,b.
(124) For Na_2F the experimental value for the vertical ionization potential is 3.85 ± 0.15 eV; see Ref. 10c.
(125) For Na_2Cl Hartree–Fock calculations yield for the vertical ionization potential 4.54 eV, $d_{Na-Cl} = 4.82$ au and for the Na–Cl–Na angle a value of 82°; see Galli, G.; Andreoni, W.; Tosi, M.P. *Phys. Rev. A*, 1986, **34**: 3580.
(126) Barnett, R.N.; Honea, E.C.; Labastie, P.; Landman, U.; Nitzan, A.; Rajagopal, G.; Whetten, R.L.; to be published.